The Nanoscale Structure of Human Female Osteoporotic Bone Investigated by Transmission Electron Microscopy

Ivan Strakhov, H. BSc.

A Thesis Submitted to the School of Graduate Studies in Partial Fulfillment of the Requirements for the Degree of Master of Applied Science

McMaster University, MASTER OF APPLIED SCIENCE (2019), Hamilton, ON

BIOMEDICAL ENGINEERING

Title: The Nanoscale Structure of Human Female Osteoporotic Bone Investigated by Transmission Electron Microscopy

Author: Ivan Strakhov, H. BSc. Biochemistry & Molecular Biology (Trent University, Peterborough, ON, Canada)

Supervisors: Dr. Henry P. Schwarcz & Dr. Kathryn Grandfield

Number of Pages: xi, 42

Lay Abstract

Human bone is a biomaterial with many levels of organization from the macroscale down to the nanoscale. The material consists of roughly 30 weight % organic components (collagen, non-collagenous proteins) and 67 weight % inorganic components (calcium phosphate minerals) deposited by bone cells. Osteoporosis is a bone disease commonly associated with increased bone porosity and bone fragility. In this study, the effect of osteoporosis on the nanoscale structure of bone was directly imaged and investigated using transmission electron microscopy (TEM). Two advanced ion milling techniques (broad beam and focused ion beam) were used to thin the bone specimens for TEM. Bioindicators relating to the structure and size of collagen and mineral components in osteoporotic versus control bone were quantified in an unbiased image analysis workflow. Findings indicated an increase in the thickness of poly-crystalline bone mineral lamellae in the nanoscale structure of human osteoporotic bone from two human donor cohorts.

Abstract

Bone is a complex hierarchical biomaterial constantly undergoing remodeling events initiated by cell signaling and fulfilled by migratory bone cells. In osteoporosis, a multitude of signaling factors cause bone resorption to proceed quicker than bone reformation, resulting in a lower bone mineral density (BMD) and porosity as seen by thinning of the cortex and trabeculae. However, the structural motifs of these altered regions of the skeleton have not been understood on the nanoscale. In this thesis, transmission electron microscopy (TEM) was used with an image analysis technique termed *nanomorphometry*, developed to enable the measurement of nanoscale structural features in human bone. Several nanoscale bone quality bioindicators relevant to the collagen fibrils and bone mineral (mineral lamellae, ML) components were defined and tested (collagen fibril diameter, interfibrillar spacing, ML thickness & ML stack thickness) among two donor cohorts of post-menopausal osteoporotic female patients and age- and sex-matched controls. In one cohort, the anatomical region investigated was the intertrochanteric crest of the femur, while in the second, the femoral neck was studied. The bone sections were prepared using an ion milling workflow yielding electron-transparent views of the bone ultrastructure. Blinded image analysis of the ultrastructure revealed that in both cohorts, the thickness of the MLs was significantly larger in osteoporotic samples versus their controls. In the former cohort, it was found that anti-resorptive drug use in the treated group did not return the ML thickness back to control levels. In the latter cohort, the ML thickness correlated more closely with the proximal femur bone mineral density (BMD) than the age of the patient. These findings suggest that the morphology of the nanoscale mineral phase is affected by osteoporosis, an effect indirectly observed by other techniques, and warrants further exploration into the implications of this effect on bone quality, fragility and strength.

Acknowledgements

Thank you to both of my supervisors, Dr. Henry P. Schwarcz and Dr. Kathryn Grandfield for opening my eyes to the some of the most thrilling bone research topics one can wish to explore. You motivated me and fostered conversations and collaborations with some of today's best scientists and engineers in biomedical research. Thank you to Dr. Cheryl Quenneville and Dr. Eve Donnelly for selection and provision of samples for this study.

To all of my colleagues in JHE A406, Grandfield Research Group and Botton's Group, thank you for making my world brighter even after dark microscopy rooms. Special thanks to GRG members Bryan Lee, Xiaoyue Wang, Joseph Deering, Dakota Binkley, Natália Marins, Chiara Micheletti, Daniel Osorio, and all the researchers who brought such revolutionary research topics in bone, microscopy and biomaterials to the table.

My sincerest thanks to the technical staff at the Canadian Centre for Electron Microscopy (CCEM) who helped and advised me in completing this project. Thank you to Carmen Andrei for the training and guidance on the TEM. Thank you to Travis Casagrande for the FIB-SEM bone section lift-outs, Jhoynner Martinez & Andy Duft for sample coating, ion milling training & advice, and Chris Butcher for the SEM training.

I would like to extend my gratitude to the McMaster Institute for Research in Aging and the Labarge Centre for Mobility in Aging for their support of this interdisciplinary project through the Catalyst Grant in 2017. Dr. Janet Pritchard, Dr. Justin de Beer, Dr. Alexandra Papaioannou and Dr. Jonathan D. Adachi are acknowledged for their collaboration for the inception of this project. Thank you to the School of Biomedical Engineering at McMaster University for welcoming a physical scientist into the school with open arms.

Finally, I would like to thank my family, friends and mentors for their caring support and interest in my research from the start. Though distance separates us, the time will come when we will meet again. A special thank you to the love of my life, Jennifer-Ann Morris, for keeping me in sound body and mind throughout any hardship.

Table of Contents

Lay Abstract……... iii

Abstract……...iv

Acknowledgements……..v

Table of Contents……vi

List of Figures……...viii

List of Tables…….. ix

List of Acronyms……. x

Declaration of Academic Achievement……..xi

Structure of Thesis……xii

Chapter 1: Introduction

1.1 Research Motivation…… 1

1.2 Research Objectives……2

1.3 The Ultrastructure of Human Bone……..2

1.4 Nanoscale Bone Quality and the Osteoporotic Pathology……...3

1.5 Ion Milling, TEM, and Nanomorphometry of Bone……4

Chapter 2: "TEM Nanomorphometry of Osteoporotic Human Bone Ultrastructure"

2.1 Abstract……9

2.2 Introduction……..9

2.3 Methods……..12

2.4 Results……16

2.5 Discussion……..17

2.6 Conclusions……19

2.7 Acknowledgements……....20

Chapter 3: "Nanoscale Bone Quality at Osteoporotic Human Bone Fracture Sites Investigated by Ion Milling and BF-TEM Nanomorphometry"

3.1 Abstract……..21

3.2 Introduction……21

3.3 Methods……..23
3.4 Results……26
3.5 Discussion……..30
3.6 Conclusions……31
3.7 Acknowledgements……31
Chapter 4: Summary & Future Directions……... 32
References……..35
Glossary of Specialized Terms…….. 42

List of Figures

Figure 1.1: Structure of bone from micro- to nanoscale.

Figure 1.2: Overview of ion milling preparation of bone specimens.

Figure 1.3: Beam diagram of a transmission electron microscope imaging in bright-field mode.

Figure 1.4: Nanomorphometry of human bone in BF-TEM micrographs.

Figure 2.1: The hierarchical, multi-scale structure of bone.

Figure 2.2: Focused ion beam site selective lift-out process from human bone.

Figure 2.3: Typical TEM image of FIB section of bone cut normal to the axes of collagen fibrils.

Figure 2.4: Definition of nanomorphometric measures

Figure 2.5: Results of blinded TEM micrograph nanomorphometry on FIB lift-outs of control, osteoporotic and bisphosphonate-treated human bone.

Figure 3.1: Human proximal femur with location selected for extraction.

Figure 3.2: ROIs imaged by BF-TEM in ion milled human bone sections for use in nanomorphometry.

Figure 3.3: Results of nanomorphometry of ML thickness in control and osteoporotic ion-milled bone sections.

Figure 3.4: Average mineral lamella thickness in each specimen studied as a function of donor age and proximal femur T-score.

List of Tables

Table 2.1: Bone samples studied with nanomorphometry.

Table 3.1: Human post-mortem donor proximal femurs selected.

Table 3.2: Bone ultrastructure nanomorphometry of control and osteoporotic human bone ion milled sections.

List of Acronyms

ACP	Amorphous Calcium Phosphate
BF	Bright Field
BP	Bisphosphonate
BMD	Bone Mineral Density
CCEM	Canadian Centre for Electron Microscopy
CCD	Charge-Coupled Device
CF	Collagen Fibril
DEXA	Dual-Energy X-ray Absorptiometry
DF	Dark Field
EELS	Electron Energy Loss Spectroscopy
FIB	Focused Ion Beam
FOV	Field of View
FTIRM	Fourier Transform Infrared Microscopy
GMS	Gatan Microscopy Suite
HC	Haversian Canal
ML	Mineral Lamellae
NCP	Non-Collagenous Protein
PFIB	Plasma Focused Ion Beam
PMMA	Poly(methyl methacrylate)
ROI	Region of Interest
SAXS	Small Angle X-ray Scattering
SD	Standard Deviation
SEM	Scanning Electron Microscopy
STEM	Scanning Transmission Electron Microscopy
TEM	Transmission Electron Microscopy
qBEI	Quantitative Backscattered Electron Imaging

Declaration of Academic Achievement

I declare that the original research work presented in this thesis was written solely by myself, Ivan Strakhov. My research supervisors, Dr. Kathryn Grandfield and Dr. Henry P. Schwarcz, conceived the project, interpreted results, and assisted with editing. Unless otherwise noted, I performed all experiments including fixing, dehydrating, embedding, sectioning, optical microscopy, polishing, dimple grinding, ion milling, SEM, TEM, image blinding, nanomorphometric analysis and statistics.

The contributions of the following researchers to completion of this thesis are declared:

- Dr. Eve Donnelly and Ashley A. Lloyd (Dept. of Materials Science & Engineering, Cornell University, Ithaca, NY) provided samples for the study presented in Chapter 2.
- Dr. Cheryl Quenneville (Dept. of Mechanical Engineering, McMaster University, Hamilton, ON) provided and advised and Cooper Gluek helped extract the specimens investigated in the study in Chapter 3.
- Dr. Janet Pritchard (Dept. of Kinesiology), Dr. Justin de Beer, Dr. Alexandra Papaioannou, and Dr. Jonathan D. Adachi (Dept. of Medicine) collaborated with Dr. Grandfield and Dr. Schwarcz on the McMaster Institute for Research in Aging (MIRA) & Labarge Centre for Mobility in Aging "Catalyst" 2017 grant to support this project. A research poster presented at the MIRA Aging Research Day & Poster Competition in December 2018 won Silver in the Master's category.
- FIB lift-out procedure on all specimens studied in Chapter 2 was completed by Travis Casagrande on a Zeiss NVision40 at the Canadian Center for Electron Microscopy (CCEM; Hamilton, ON).
- Carbon coating for all SEM & TEM samples was provided by Jhoynner Martinez at CCEM.
- Glutaraldehyde fixative solution was provided by Marcia Reid (McMaster Faculty of Health Science Electron Microscope Facility).

Chapter 1: Introduction

1.1 Research Motivation

Osteoporosis is a multifactorial disease that has been defined and diagnosed in humans as a bone mineral density (BMD) of greater than -2.5 standard deviations (SD) away from the mean BMD of a healthy sex-matched adult [1]. This measure is referred to as the T-score. It is measured clinically by dual energy X-ray absorptiometry (DEXA) usually of the central skeleton (hip and spine, two common sites of osteoporotic fracture) in order to evaluate and monitor osteoporosis progression, fracture risk and drug-treatment response [2].

There are many tools (microscopy, spectrometry, tomography, etc.) available to study bone material. Bone material from animal models of osteoporosis and from donors has been used to study the composition and structure of bone on the nanoscale; however, these have always been imaged/quantified over micron scale distances or larger. Transmission electron microscopy, a technique that can achieve atomic resolution must be used in order to image directly the nanoscale structure (or "ultrastructure") of bone, after which image analysis software may be used to quantify bioindicators within the bone tissue. The bone tissue must be prepared in a way that preserves the original ultrastructure as it would be present in the bulk *in vivo* specimen. Past studies that prepared bone for TEM, (which requires a sample thickness of < 200 nm to be electron transparent), used ultramicrotomy which has been shown to break the mineral component of bone ultrastructure prior to TEM imaging [3], [4]. Ion milling, which slowly polishes the sample thickness with an ion beam has shown promising results for preserving bone ultrastructure. The true ultrastructure of osteoporotic versus control bone on the nanoscale has scarcely been imaged and/or understood.

The morphology and interplay between the main ultrastructural components (collagen fibrils and mineral lamellae) in osteoporotic versus control bone must be determined in order to characterize osteoporosis from a biomaterial standpoint. The material structure of osteoporotic bone on the nanoscale has important implications for anti-osteoporosis drug-treatment, specialized bone implant designs and the definition of the disease.

1.2 Research Objectives

This thesis aims to investigate and understand the bioindicators for osteoporosis (OP) at the nanoscale using transmission electron microscopy of ion milled sections. More specifically, the discrete objectives of this work were:

- Isolate bone biomaterial from bulk bone specimens from osteoporotic fracture regions of control (non-OP) and osteoporotic bone from proximal femurs.
- Prepare focused ion and broad ion beam milled sections of human osteoporotic and control trabecular or trabecularized bone.
- Image representative regions of the bone ultrastructure in control and osteoporotic bone samples at high magnifications using bright-field TEM.
- Quantify and compare nanomorphometric bioindicators (ML and ML stack thickness, collagen fibril diameter, and interfibrillar distance) of nanoscale bone quality in TEM micrographs using a blinded image analysis workflow.

If significant changes in the tested bioindicators in osteoporotic bone ultrastructure of collagen and mineral components were found, these should be further investigated by other nanoscale microscopic and spectroscopic techniques to determine changes to bone material ultrastructure during aging and osteoporosis.

1.3 The Ultrastructure of Human Bone

The ultrastructure of bone is comprised of two main features: collagen fibrils and mineral lamellae (ML). Collagen fibrils (CFs), roughly 50 nm in diameter and hundreds of nm long [3], [5], [6], are comprised of aggregated tropocollagen triple-helices. These CFs are arranged co-planarly during bone matrix deposition by osteoblast cells into lamellar layers which form the basis for the alternation of CF alignment in adjacent layers of hemiosteonal (in trabeculae) and osteonal (in cortical osteons) lamellae (Figure 1.1). Between the collagen fibrils, with roughly equivalent volume fraction percent in the ultrastructure, lie stacks of mineral lamellae (MLs). There has been much debate over recent years about the “true” structure of MLs, primarily whether they are needle- or plate-like, but proponents of either argument agree that they are poly-crystalline apatite (calcium phosphate) mineral structures that surround and follow the length of collagen fibrils, with the *c* axes of the crystals roughly aligned with the longest axis of

the ML and/or CF. Other components (with low vol% and wt%) present in the ultrastructure are amorphous calcium phosphate (ACP), thought to be an apatite crystal precursor [7], non-collagenous proteins (NCPs) have multiple functions ranging from structural [8] to mineralization-inhibitory/promoting [9], proteoglycans and water.

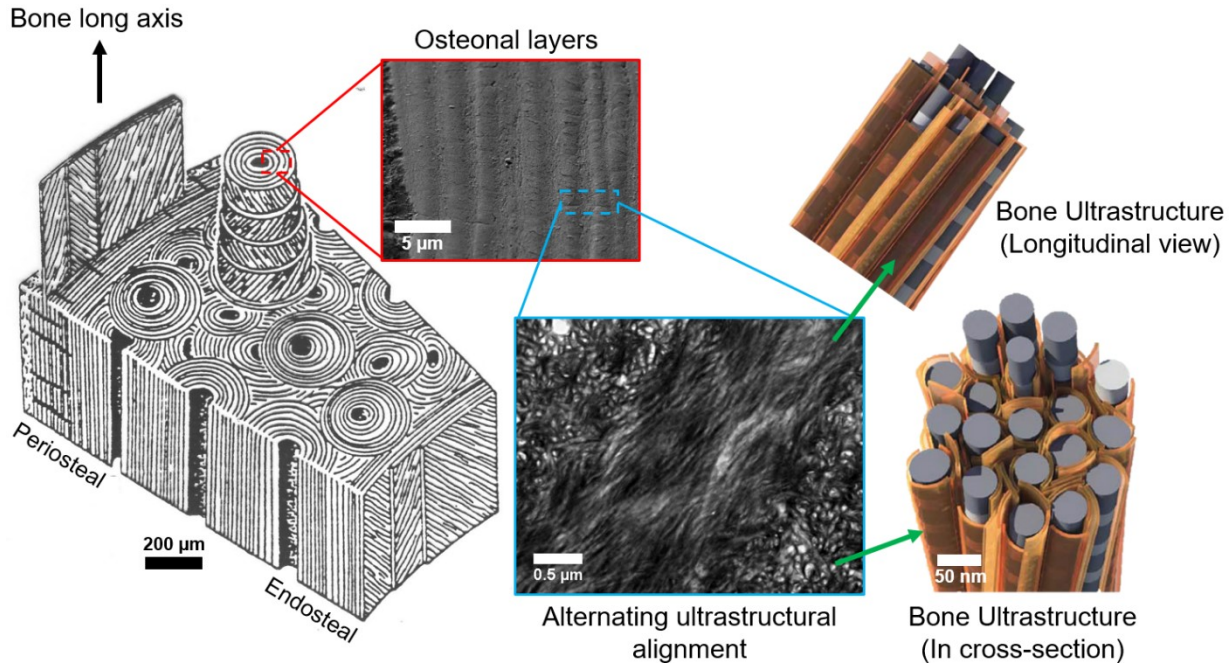

Figure 1.1: Structure of bone from micro- to nanoscale. Osteons (and hemiosteons) are concentric layers of mineralized bone matrix (red), that alternate in CF and ML alignment (blue) forming two ultrastructural motifs on the nanoscale (green). Adapted from [10], [11].

The above components are involved in the nanoscale structure but their arrangement has larger implications for the hierarchical structure of bone at larger levels of organization. Adjacent (hemi-) osteonal lamellae alternate in CF alignment (resulting in the "twisted-plywood" [10] arrangement of bone) which helps to slow crack propagation through multiple layers. The mineral lamellae mineralize in the extrafibrillar space wrapped tightly around adjacent hexagonally packed CFs. Proteoglycans play an important role in bone toughness [12]. Changes in one or multiple of these ultrastructural parts could likely have an effect on the behaviour of bone material as a whole, across large ranges in the skeleton. Do any changes in bone ultrastructure occur during degenerative bone disease, such as osteoporosis? If so, can we detect these changes first-hand using high-resolution electron microscopy imaging techniques? Where in the skeleton do we look for signs of osteoporosis?

1.4 Nanoscale Bone Quality and the Osteoporotic Pathology

The changes in bone structure and matrix composition on a variety of length scales in osteoporosis and other degenerative bone diseases is termed "bone quality". The term encompasses a variety of bioindicators that describe an increase in bone's ability for stable remodeling, stress dissipation and micro-structural integrity, all of which contribute to bone strength and reduce fracture risk [13], [14]. The term has been extended to nanoscale or material bone quality indicators, some of which measure: bone matrix mineralization [15], [16]; mineral morphology [17]; mineral composition [18]–[20]; collagen cross-linking [21], banding [22]; nanoscale tissue strength [23]; and mineral-to-matrix ratio and maturity [24]. These features all pertain to bone quality at the ultrastructural level of bone; however, a lot of the techniques used have a micro-meter level probe size, and do not image the ultrastructure directly. Fourier transform infrared microscopy (FTIRM) studies of bone can achieve 6 μm spatial resolution [20]. Small-angle X-ray (SAXS) is capable of 20 μm pixel size [25]. These techniques are sometimes combined together for nanoscale bone ultrastructural analysis [26] or with quantitative backscattered electron imaging in the scanning electron microscope (qBEI-SEM) for microscale tissue mineral density contrast [16].

Osteoporosis has been defined by the World Health Organization (WHO) as a bone mineral density (BMD, in g/cm^3) of more than 2.5 SDs (standard deviations) below the mean BMD of a healthy, sex-matched adult population [1]. The presence of a fracture, especially in common regions of osteoporotic fracture (the hip, spine and wrist), is also diagnostic [1]. BMD does not appear to explain all incidences of fracture, or be the sole factor in bone strength, fragility and fracture risk [27]. Micro-mechanical and micro-architectural characteristics have been found to describe bone fragility much better than BMD [28]. Hence, the above bone quality indicators are used to describe the quality of the nanoscale structure and material characteristics of osteoporotic bone. Osteoporosis is a disease of runaway remodeling by increased osteoclast activity, which can result in porous bone. The effect is highly accelerated in post-menopausal women, due to reductions in systemic estrogen [29]. The endocortical region of bone affected by osteoporosis takes on a "trabecularized" appearance with large Haversian canals (HC), highly remodeled endocortical surface, and reduced trabecular network [30]. Patients are commonly prescribed anti-resorptive (e.g. bisphosphonates) therapies to reverse these effects by promoting

new bone formation and reducing bone resorption in cases of post-menopausal osteoporosis [31]. Less commonly they are prescribed anabolic drugs (e.g. parathyroid hormone) [32]. These treatments can result in increased mineralization and reduced mineralization heterogeneity of the bone architecture, as observed by qBEI-SEM [15] and in the overall increase of bone mineral density on the macroscale as measured by DEXA. The regions of defective bone microarchitecture and the osteoporotic fracture regions listed above are of interest as indicators of recent influence of osteoporosis. This thesis specifically studies two different post-menopausal osteoporotic bone donor cohorts (and their age-matched controls), using bone from the proximal femur, with matching anatomical regions and preparation of microarchitecturally-similar regions of interest (ROIs) for nanoscale TEM imaging. Several bioindicators of bone ultrastructural quality were defined and measured: ML thickness, ML stack thickness, collagen fibril diameter, and interfibrillar spacing.

1.5 Ion Milling, TEM, and Nanomorphometry of Bone

Imaging bone in the TEM requires that the bone is below 200 nm in thickness to be electron transparent. This can be easily achieved using ultramicrotomy (diamond knife sectioning) which is primarily what has been used to prepare thin bone sections for TEM in the past. However, it has been shown in multiple studies of mineralized bone tissue that ultramicrotomy is destructive to bone ultrastructure [4], [33] in that it breaks mineral lamellae around collagen fibrils. A technique that is "gentler" to the ultrastructure of bone, and is being increasingly used for bone TEM specimen preparation is ion beam milling [3], [34], [35], which keeps the MLs intact, as they would be in the native bone specimen. There exist three primary ion beam milling techniques for preparing bone: broad ion milling, focused ion-beam (FIB) milling, and plasma focused ion-beam milling (PFIB). The latter technique, which polishes bone using Xenon ions, is currently being applied for large field-of-view (FOV; 50 µm x 50 µm) serial sectioning and tomography of human bone. The former two techniques have been established as suitably non-destructive to bone ultrastructure, relatively inexpensive, and site-selective, which is important for osteoporotic bone sample preparation for TEM.

In the two studies presented herein, gallium FIB and broad beam argon ion milling were used to prepare electron transparent samples of bone for TEM. Focused ion beam milling is useful for site-selective lift-outs (measuring roughly 10 x 10 x 0.2 µm in *l* x *w* x *t*) from the bulk

bone sample surface (Figure 1.2A). This ability can be employed to study specific lamellar layers within either trabecular or cortical bone, for example. Gallium FIB was used to prepare *in situ* lift-outs from trabecular and trabecularized [30] bone from recent remodeling events to look for evidence of osteoporosis on the nanoscale. Ion milling was applied to trabecular ROIs from bulk sections of osteoporotic bone. In ion milling, a low-angle argon ion beam mills the center of a bone sample until a hole is formed (Figure 1.2B). The material on the edges of this hole (radially about 100 µm) is electron transparent, and affords a large imaging area of bone ultrastructure. The voltage and current of the argon ion beam used were based on recommended tables for ion milling of soft materials and ceramics. Figure 1.2, shown below, details the two techniques.

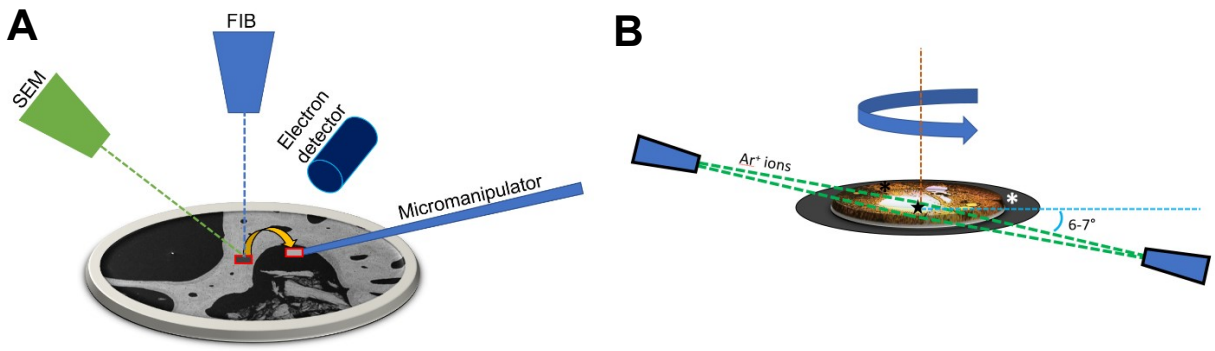

Figure 1.2: Overview of ion milling preparation of bone specimens. A) FIB milling *in situ* lift-out procedure; a micromanipulator extracts a thin bone section milled by the Ga^+ ion beam from the surface of the specimen. B) Ion milling procedure, whereby a broad, low-angle Ar^+ beam mills the center of a rotating sample until the material is electron transparent.

Transmission electron microscopy (TEM) is a nanoscale imaging technique that has been used to image human bone [5], [36], [37] and animal bone [38] and other mineralized tissues [39], [40]. The two studies herein use bright field TEM (Figure 1.2 for beam diagram) which is well suited to resolving the morphology of individual apatite crystals, due to diffraction and mass-thickness contrast allowing high resolution of single mineral particles. The mineral lamellae scatter strongly and appear as dark crystalline features while adjacent collagen fibrils appear lighter and show the characteristic 67 nm d-period of gap and overlap zones. In bright-field (BF) mode, the cross-sectional (CS) and longitudinal motifs [5], [37] of bone ultrastructure are apparent. In images of CS regions in bone, the thickness of mineral lamellae can be easily quantified. Past studies using ultramicrotomy to section bone were able to identify hydroxyapatite crystals in BF-TEM [38], [41]. Ion beam milling of bone has also shown promise for preparing TEM specimens with intact hydroxyapatite crystals. For TEM of soft materials

such as bone, a low voltage (30-200 kV) should be used to prevent electron beam damage [42]. The dwell time should also be reduced during imaging. This will prevent sample damage by heating [43]. A thin (< 50 nm) layer of carbon is often used as a sacrificial layer to the electron beam in the TEM. BF-TEM images of bone ultrastructure can be analyzed in post-processing using nanomorphometry.

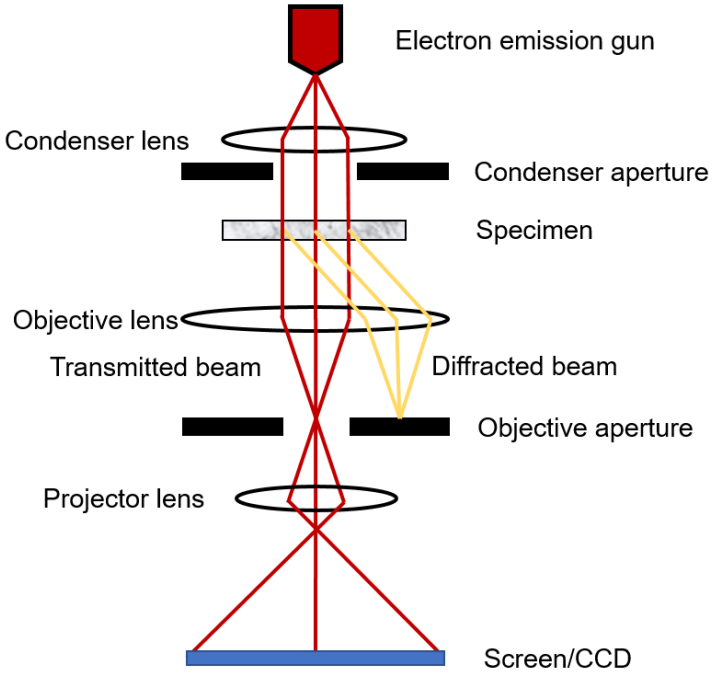

Figure 1.3: Beam diagram of a transmission electron microscope imaging in bright-field mode (adapted from [44]). A parallel electron beam interacts with the thinned bone specimen. Areas of high density or thickness, as well as crystalline areas, diffract strongly, are blocked by the objective aperture and appear as regions of darker contrast in the image. Less thick/dense regions have lower mean free path through the specimen, transmit the electron beam more freely, and appear as regions of lighter contrast.

Nanomorphometry (similarly to histomorphometry) is the term for quantification of ultrastructural features in bone tissue using image analysis software (Photoshop, ImageJ/Fiji, GMS, etc.). Although this technique has been applied to quantification of collagen and mineral features in human bone in the past [5], [11], comparisons of ultrastructural measures between healthy and osteoporotic bone have never been done before the present study. For this purpose, an image blinding script in Fiji [45] was used to remove associable labels (storing in a log file) from a batch of BF-TEM images originating from osteoporotic and control bone samples.

Mineral lamella thickness, ML stack thickness, CF diameter and interfibrillar distance were the bioindicators quantified by nanomorphometry. The associated log file was then "unblinded" and the bioindicator data organized by bone sample origin and group. Significant differences between groups were determined using a t-test ($p < 0.05$) with Welch's correction. The features measured by nanomorphometry were proposed as bioindicators of the nanoscale structural quality of human bone tissue.

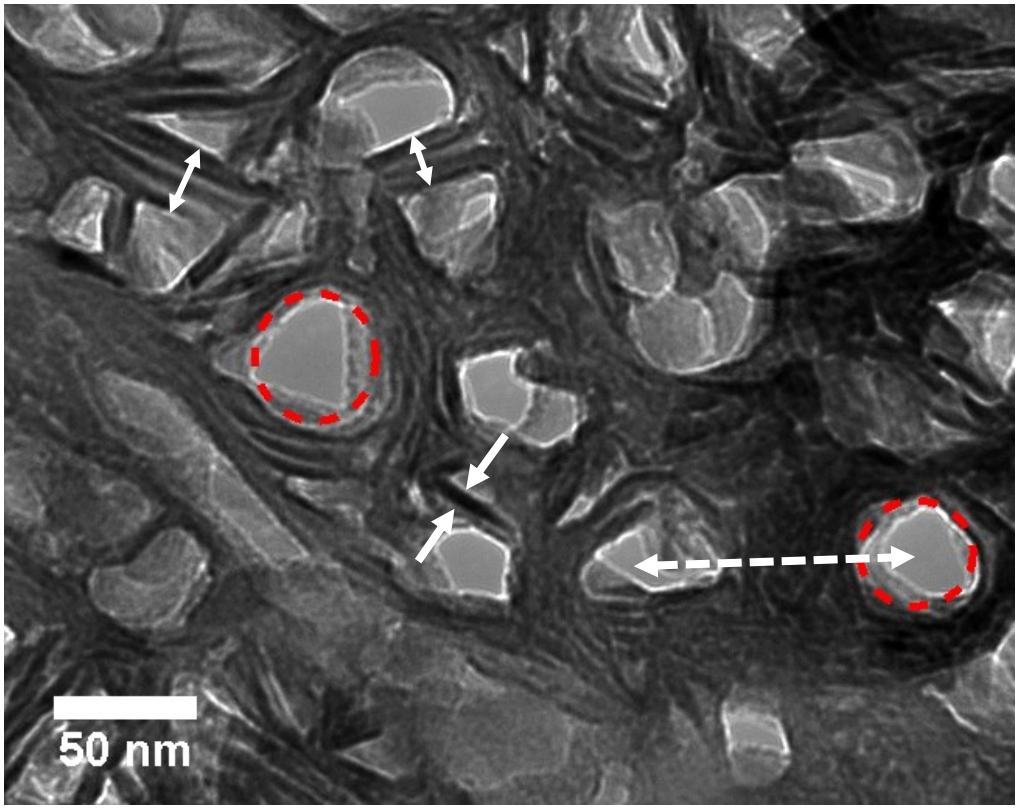

Figure 1.4: Nanomorphometry of human bone in BF-TEM micrographs as defined in this thesis. The 4 indicators are: ML thickness (between solid white arrows), ML stack thickness (double headed arrows), CF diameter (red circle), and interfibrillar distance (dashed double headed arrow) are quantified in a blinded image library of human bone ultrastructure with image analysis software.

Chapter 2:

TEM Nanomorphometry of Osteoporotic Human Bone Ultrastructure

2.1 Abstract

The true arrangement of human bone on the nanometer scale, termed the ultrastructure, made up of collagen fibrils and calcium phosphate mineral lamellae, is clearly imaged using transmission electron microscopy (TEM) of ion-beam milled sections of bone. The way that osteoporosis manifests itself in the nanoscale organization of human bone has been sparsely studied using TEM. Focused ion beam (FIB) milling was used to prepare specimens of osteoporotic bone, osteoporotic bisphosphonate (BP)-treated bone, and bone from age-matched controls for high magnification bright-field TEM imaging. Quantitative image analysis was used to study nanoscale bone quality indicators pertinent to mineralization. This method, called nanomorphometry (analogous to histomorphometry), can only be applied to ion-beam-milled sections such as those used here. The thickness of poly-crystalline mineral lamellae) was significantly increased, additionally the spacing between collagen fibrils was significantly reduced in osteoporotic bone groups. No significant change was found in the thickness of stacks of mineral lamellae between collagen fibrils. These direct imaging results support small angle X-ray scattering based findings in the literature that the dimensions of the individual mineral particles of bone are increased in the osteoporotic pathology.

2.2 Introduction

Bone is a composite biomaterial made of organic protein (collagen type I & other non-collagenous proteins; “NCPs”) and inorganic crystalline apatite mineral. Collagen type I triple helices are assembled in the form of fibrils (CFs) that are roughly 50 nm in diameter and hundreds of nm long. Due to their nanostructure, they typically display a 67 nm [46] periodicity of gap and overlap zones. TEM Imaging of ion milled sections of bone reveals that most of the mineral phase lies outside of and encases the CFs [5], although the gap zones of the CFs also contain calcium phosphate [35], [47]. The MLs are poly-crystalline plates of apatite (calcium phosphate) with the *c*-axis of the apatite crystals quasi-aligned along the length of the CFs [35], [48]. Bone is known to be a hierarchical biomaterial due to its multi-level organization [35], [49] (Figure 2.1) which contributes to its toughness. The mesoscale arrangement of bone (osteonal &

hemi-osteonal layers) has been claimed to contribute to toughness by slowing crack propagation, but only a few studies have investigated how the nanoscale structure and composition of bone affects strength and toughness of bone [6], [50], and this is crucial to understanding bone pathologies such as osteoporosis, which present clinically with increased fragility and fracture risk [13], [51]. Osteoporosis is defined by the WHO as a reduction of one's bone mineral density (BMD) to more than 2.5 standard deviations below the mean BMD for one's sex and age group [1]. While BMD is the standard for clinical diagnosis, patients with normal BMD still suffer osteoporotic fractures, suggesting that the disease manifests multi-factorially and other bioindicators that are altered in osteoporotic bone may affect the fragility and strength.

Many characteristics of bone have been investigated to study the effects of osteoporosis, collectively referred to as "bone quality". These characteristics may be determined using microscopic and spectroscopic methods if the bone is preserved from specific anatomical locations known to be affected by osteoporosis. For instance, endosteal remodeling in post-menopausal osteoporosis destroys the trabecular network and produces trabecularization or porosity of the cortex [30]. The (hemi)-osteonal layers formed by osteoblasts at these sites contain bone that was formed during the time that the person was osteoporotic. These osteoporotic trabecular and endocortical regions were the focus of this work. In osteoporotic bone, in addition to the loss of whole-bone or whole-body bone mineral density (BMD), there is a loss of nanoscale mineralization maturity and heterogeneity [15], [16]. The morphology of the mineral crystallites on the nanoscale has been reported to be affected by osteoporosis [17], [52], with crystal dimensions (mineral lamella thickness, width and length) increasing in osteoporotic bone and more specifically at peri- and endosteal bone regions. The collagen d-periodicity distribution has been shown to fluctuate in osteoporotic bone [46]. Glycosaminoglycans, structural NCPs, become scarce with age [12]. In studies of bone from sustained fractures in post-menopausal women using Fourier Transform Infra-Red Micro-spectroscopy (FTIRM), reduced carbonate substitution and collagen cross-linking maturity [53], in addition to increased mineral crystal size [54] were associated with propensity to fracture. While these studies show the importance of nanoscale ultrastructural components to bone quality, the interplay between and changes in the organic and inorganic building blocks of osteoporotic bone has never been imaged directly.

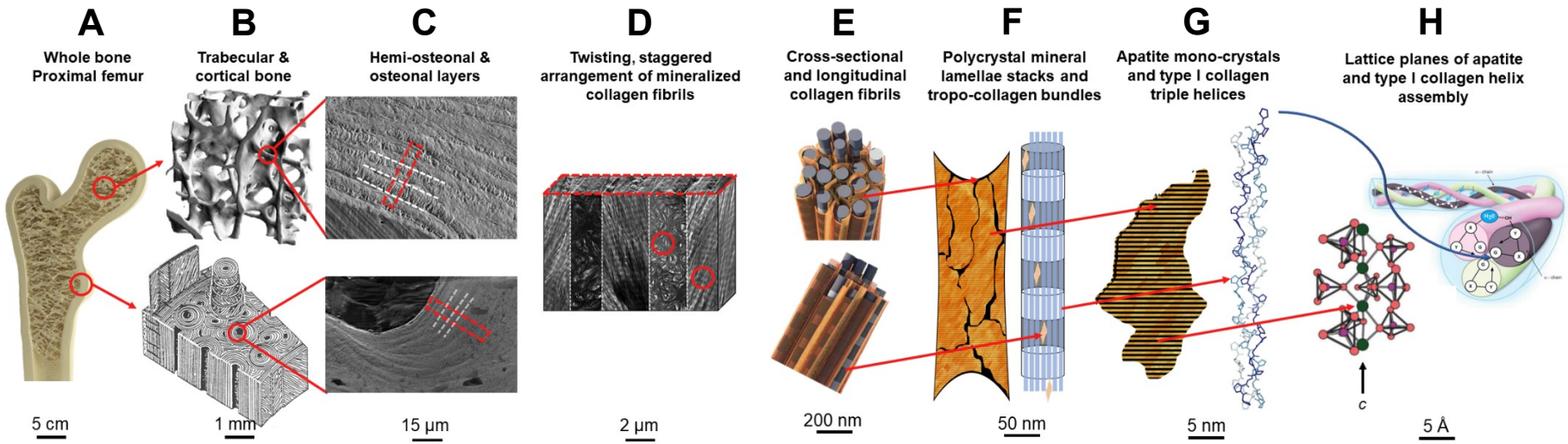

Figure 2.1: The hierarchical, multi-scale structure of bone. A) A whole bone (proximal femur) which is sectioned to show the inner network of trabecular (from [55]) and outer shell of cortical bone (from [10]). B) The porosity of trabecular bone arising from its strut-like bridging features (top), and the striated layered structure of cortical osteonal bone (bottom). C) Hemi-osteonal (from trabecular, top) and osteonal (from cortical, bottom) layers of bone from cellular remodeling events. D) Successive layers of (hemi-/) osteonal bone contain mineralized collagen fibrils, which change direction between layers following a twisting pattern throughout. E) Collagen fibrils are seen in two orientations mainly; cross-sectional (top) and longitudinal (bottom). Fibrils are usually 50 nm in diameter, hundreds of nm long, with a gap-overlap d-periodicity of about 67 nm. They are mineralized interfibrillarly by polycrystalline mineral lamellae (from [11]). F) Mineral lamellae are found between fibrils as curved crystal stacks that are aligned in their largest dimension to the length of the collagen fibrils. Some authors state that the gap zone contains some nucleating mineral crystallites. G) Individual crystals of carbonated hydroxyapatite make up a mineral lamella. The collagen fibrils are made up of bundles of tropocollagen molecules (from [56]). H) The apatite crystals (from [57]), aligned with the *c* axis roughly parallel to the fibril long axis, have a hexagonal lattice structure with multiple dislocations, defects and substitutions. The tropocollagen molecules are triple helical amino acid assemblies.

The collagen d-periodicity distribution has been shown to fluctuate in osteoporotic bone [46]. Glycosaminoglycans, structural NCPs, become scarce with age [12]. In studies of bone from sustained fractures in post-menopausal women using Fourier Transform Infra-Red Micro-spectroscopy (FTIRM), reduced carbonate substitution and collagen cross-linking maturity [53], in addition to increased mineral crystal size [54] were associated with propensity to fracture. While these studies show the importance of nanoscale ultrastructural components to bone quality, the interplay between and changes in the organic and inorganic building blocks of osteoporotic bone has never been imaged directly.

Patients with osteoporosis are commonly prescribed a class of anti-resorptive drugs called bisphosphonate (BP) that act to decrease the activity of osteoclasts, and have been shown to increase BMD and prolong secondary mineralization [31], [58]. Roschger et al showed using backscattered electron intensity of the micro-scale surface of a bone specimen (the qBEI method) that weight % of calcium in bone following BP therapy was more heterogeneous, as well as the degree of mineralization (average Ca wt%) was increased, while the Ca wt% in osteoporotic bone was significantly reduced [15].

The primary reason for the lack of clarity in some previous studies of bone ultrastructure (osteoporotic or not) with TEM is the sample preparation method. Ultramicrotomy of bone destroys the ultrastructure by breaking mineral lamellae. A preferable technique that is increasingly implemented [5], [11], [37], [59] is ion beam milling , either using the ion-mill [5], [11] or focused ion beam (FIB) milling [37], [49], which are capable of keeping the ultrastructure intact closer to what it would look like in the native environment.

In this study, we use FIB sectioning to prepare lift-outs from polished sections of osteoporotic, osteoporotic +BP-treated, and control human bone for TEM imaging. Nanometer-scale structural features of trabecular and trabecularized cortical bone are resolved, quantified and compared through a modified version of histomorphometry as applied to nanoscale features, which we call *nanomorphometry*.

2.3 Materials & Methods

Specimens: Six human bone specimens (N = 2 in each group) (Table 2.1) were received with institutional ethics board approval. Specimens were previously extracted during an

intertrochanteric crest fixation nail procedure (or a biopsy for control patients) from the proximal anterior femur, as described earlier [23]. Specimens were analyzed as received in embedded blocks of poly(methyl methacrylate) (PMMA) that had been polished to allow extraction of FIB sections. Three groups of samples were contrasted: controls; osteoporotic (OP); and osteoporotic patients who had been treated with bisphosphonates (OP +BP-treated).

Table 2.1: Bone samples studied with nanomorphometry

Group	Fracture?	Age/Sex
Control	N	65 / F
	N	74 / F
OP	Y	85 / F
	Y	85 / F
OP +BP	Y	88 / F
	Y	58 / F

Sample preparation by FIB: The specimens were mounted onto scanning electron microscopy (SEM) stubs, and sputter coated with carbon. They were imaged on a JEOL 6610LV SEM, operated at 5 kV accelerating voltage, in back-scattered electron and secondary electron imaging mode to obtain topography and atomic number (Z)-sensitive images which were compiled into mosaics. The sample surfaces were surveyed for regions of interest (ROI) for sample lift outs and sites of trabecular or trabecularized bone were selected. Specifically, hemiosteonal layers near the medullary space were the primary ROI since these would have been formed most recently in the patient's bone, and would thus contain bone formed more closely to the time the patient was osteoporotic. The samples were then taken to a Zeiss NVision40 gallium focused ion beam (FIB) instrument for site-selective sectioning. The process is outlined in Figure 2.2 below. The lift-out plane was oriented across (perpendicular to) multiple osteonal/hemiosteonal bone deposits in order to capture different collagen/mineral orientations in the lift-out. The lift-out was attached to a copper sample grid and polished with the ion beam to below 200 nm thickness. The final dimensions of the electron transparent regions of the lift-out were about 8 x 8 x 0.2 µm.

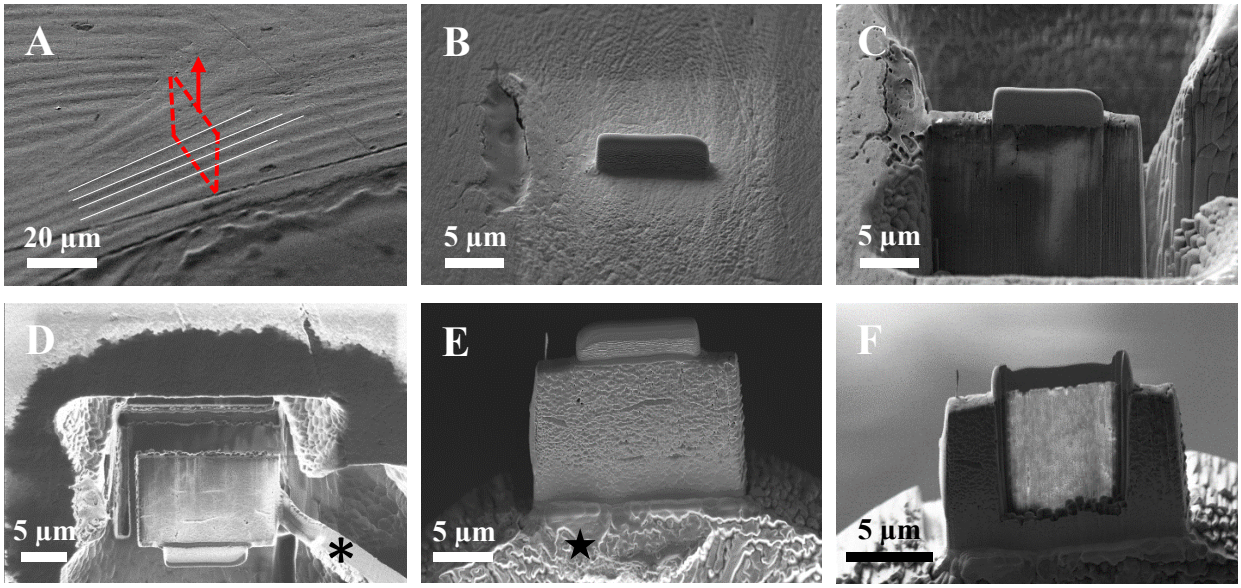

Figure 2.2: Focused ion beam site selective lift-out process from human bone. A: The lift-out plane relative to the osteonal lamellae (white lines, bordering alternating orientations of collagen fibrils) marked in red. B: It was shielded with a capping layer of tungsten. C: The surrounding region was milled using a preset milling pattern in the Zeiss NVision40. D: A micromanipulator (black asterisk) extracted the lift-out from the bulk material. E: The lift-out was attached to a copper grid (black star) for TEM. F: The FIB polished the sample to below 200 nm thickness.

Transmission electron microscopy: The lift-outs were imaged in a JEOL 2010F scanning transmission electron microscope, operated at 200 kV accelerating voltage, in bright-field mode using a double-tilt holder. Overviews of the liftouts were acquired at low magnification. Magnifications of greater than 300,000x were used to resolve ultrastructural features for analysis, such as cross-sectional regions of mineralized fibrils in the liftouts (Figure 2.3). The images were stripped of all associable labels using a blinding macro [60] in ImageJ (NIH).

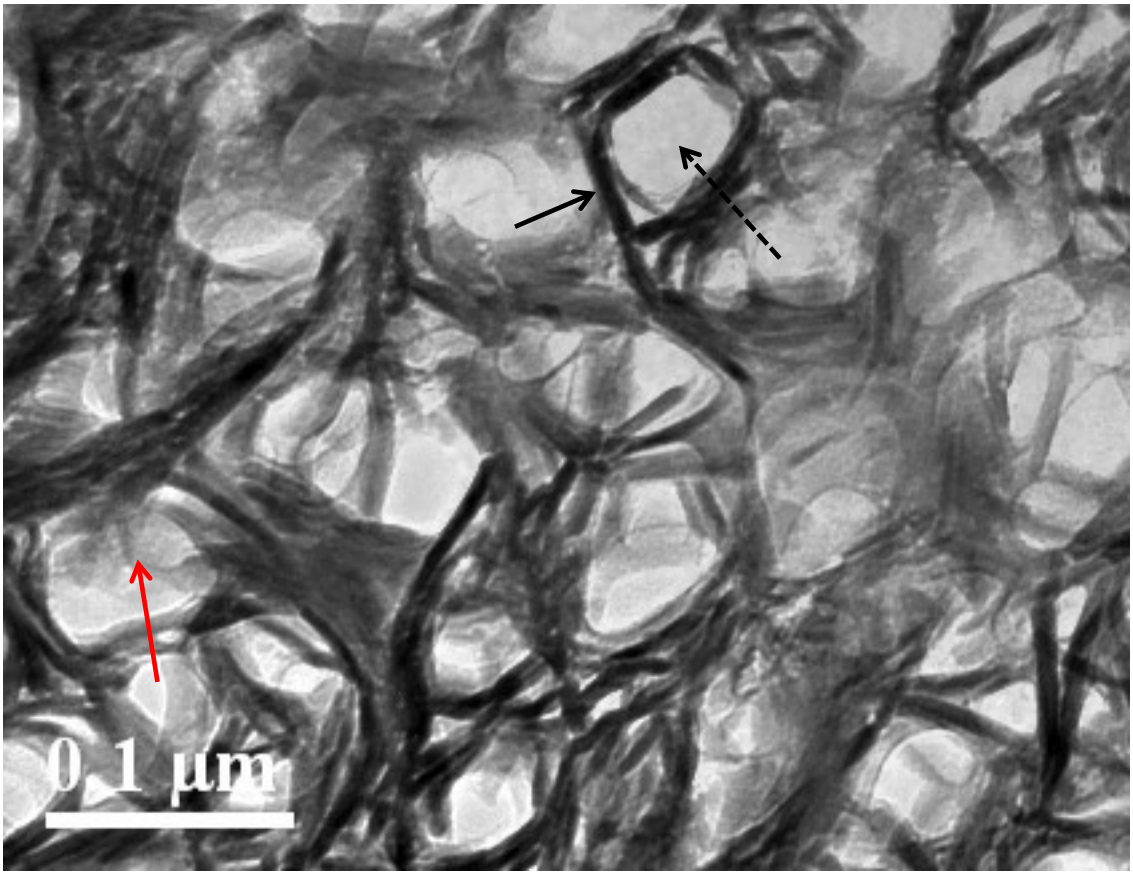

Figure 2.3: Typical TEM image of FIB section of bone cut normal to the axes of collagen fibrils. Solid arrow: edgewise view of apatite lamella wrapping around collagen fibril; dashed arrow: hole, formerly site of collagen fibril, subsequently eroded by ion beam; solid red arrow: collagen fibril with some collagen preserved in hole.

Nanomorphometry: All sections cut normal to the axes of collagen fibrils have a similar "lacy" appearance (Figure 2.3) in which hole-like features are surrounded by stacks of MLs viewed edgewise. The holes are in fact the sites of cross sections of collagen fibrils in which, in ion-beam milled sections, almost all the collagen has been eroded away by the ion beam [61]. For the purposes of comparing and contrasting such images we have identified dimensional characteristics of fields of view of such cross sections, as follows: mineral lamellae thickness, ML stack thickness (bounded by MLs between adjacent CFs), interfibrillar distance and CF diameter (Figure 2.4). We refer to these as *nanomorphometric* measures, analogous to histomorphometric measures. [62]. They can be measured manually using Fiji [45] software. After analysis, the measured indicators for each sample were unblinded using the generated index file and organized by sample group (control, OP, and OP+BP-treated).

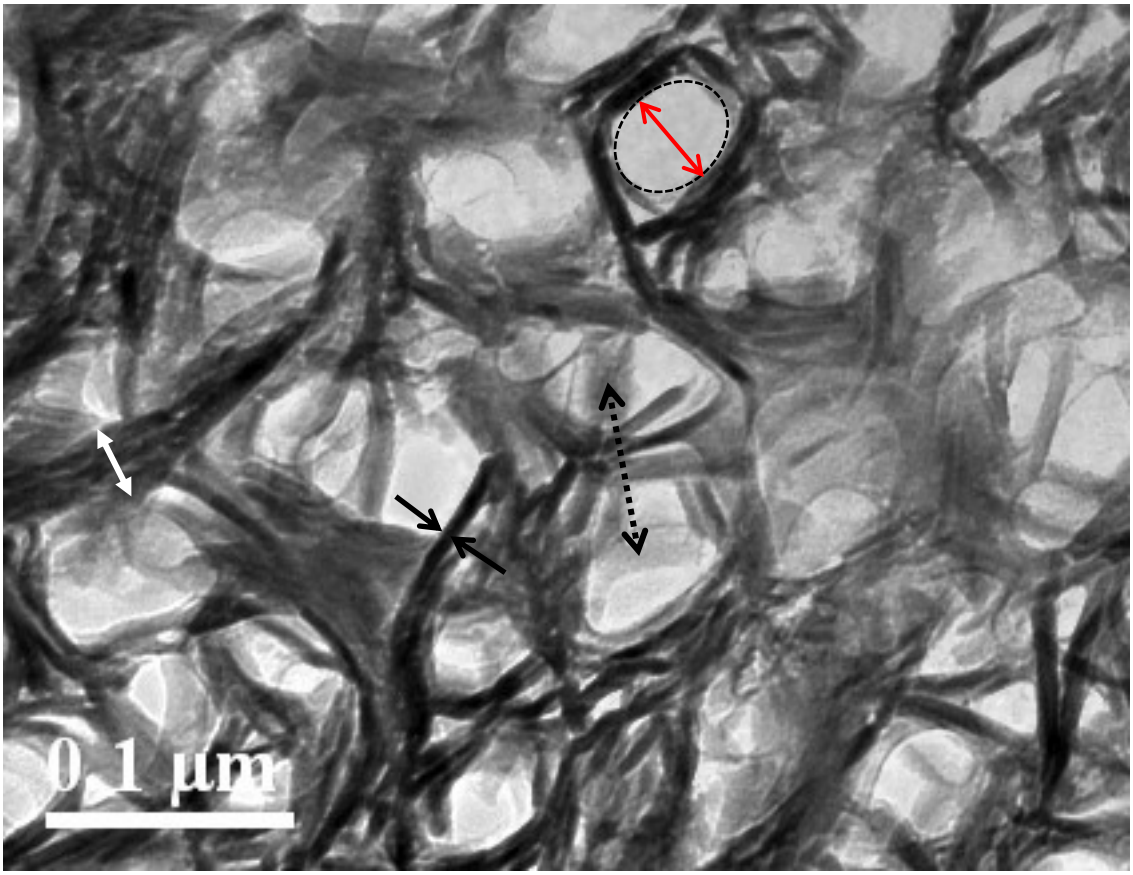

Figure 2.4: Definition of nanomorphometric measures: solid arrows: thickness of MLs; solid white double-headed arrow: ML stack thickness; dashed double-headed arrow: interfibrillar distance; solid red double-headed arrow: fibril minor diameter (measured at narrowest diameter to correct for effect of tilt).

Statistics: Preliminary power analysis on a non-blinded dataset revealed that >200 (for ML thickness) and >25 (other indicators) measurements for each nanomorphometric indicator were required to achieve >85% power within a specimen analyzed. F-test for Variance and Welch's t-test ($p<0.05$) were performed on datasets to test differences between groups.

2.4 Results

The mean, median, and distribution of each nanomorphometric indicator is shown below in Figure 2.5 as a box-and-whisker plot (as quartiles). The ML thickness was found to be significantly increased in osteoporotic and bisphosphonate-treated osteoporotic bone versus control bone, from 5.3±1.4 nm to 6.0±1.5 nm, a 13% increase in thickness. The ML stack thickness was not significantly different in any of the groups, while the interfibrillar distance in

osteoporotic bone was significantly reduced relative to controls, from 64±20 nm to 52±16 nm, a 21% reduction. No significant difference between groups was found in CF diameter.

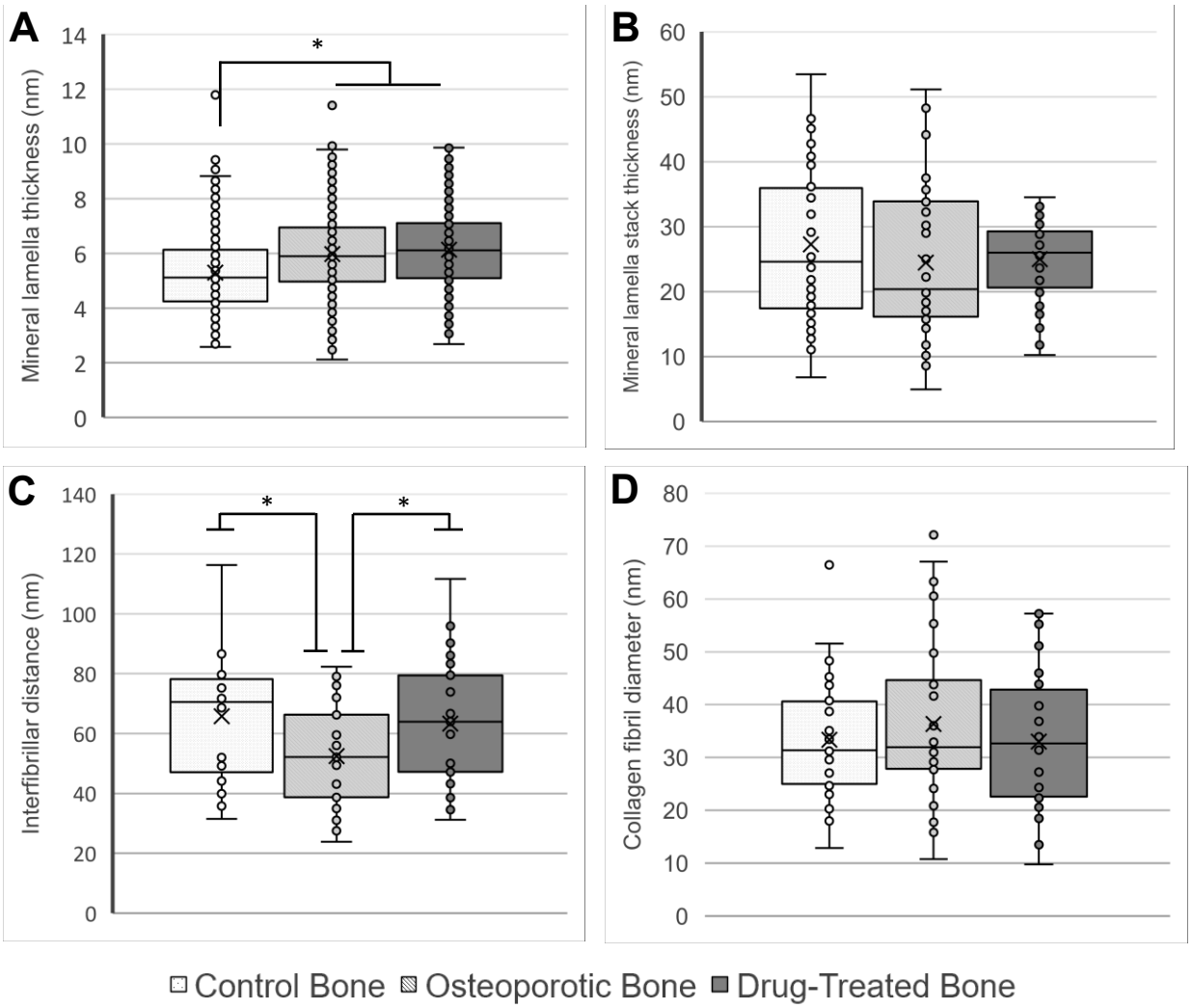

Figure 2.5: Results of blinded TEM micrograph nanomorphometry on FIB lift-outs of control (stippled), osteoporotic (diagonal lines) and bisphosphonate-treated (grey) human bone. Statistical test is t-test ($p<0.05$) with Welch's correction. A: Thickness of mineral lamellae is significantly increased (+14%) in osteoporotic and bisphosphonate-treated osteoporotic bone. B: No significant differences in stack thickness among groups. C: Interfibrillar distance was significantly reduced in osteoporotic bone relative to control (-21%) and bisphosphonate-treated bone. D: No significant change in collagen fibril diameter between control, osteoporotic and treated groups.

2.5 Discussion

The change in mineral lamellae thickness due to osteoporosis is an effect that has been observed previously in the study of bone ultrastructure (also referred to as mineral particle size or plate thickness). Studies using small-angle X-ray scattering (SAXS) have found significant increases in the mineral lamella thickness in a rat model of female post-menopausal osteoporosis [16], [17], as well as in fracture models proximal to the site of femoral fracture [63]. However, SAXS seems to consistently estimate ML thickness values much smaller than nanomorphometry. This is the first time that an increase in ML thickness has been demonstrated in human osteoporotic bone compared with specimens from the same anatomical site in control and BP-treated osteoporotic bone.

Osteoporosis is defined by a reduction of mineral density in whole bone, but its effect on the density of the bone matrix is poorly known. The majority of the mineral in bone is located in the extrafibrillar spaces [5], [11], [48]. If osteoporosis were also associated with a decrease in density of the bone matrix, then we would have expected a reduction in the thickness of stacks of mineral lamellae at the nanoscale. Perhaps, this indicates that a reduction in BMD occurs over larger volumes of bone, or at higher order hierarchical levels only, e.g. thinning of the trabeculae and the cortex [30].

There appears to be a reduction in the heterogeneity of the ML stack thickness data obtained from the bisphosphonate-treated bone, as noted by the narrower distribution of the +BP-treated group in Figure 2.5B. This effect could be due to the small sample size investigated in this work. However, a related effect is also observed by Roschger et al [15] in the study of nanoscale mineralization distribution in human osteoporotic bone using qBEI where the mineralization distribution (Ca wt%) of bone biomaterial is more homogeneous following bisphosphonate therapy.

Interfibrillar distance between CFs was significantly reduced in the osteoporotic samples relative to control and bisphosphonate-treated bone samples. This effect contrasts with the non-significant ML stack thickness result observed in Figure 2.5B in that it is not solely dependent on the interfibrillar mineralization of CFs, but may also depend on the characteristics of the bone matrix (osteoid) deposited by osteoblasts. Reductions in the distance between CFs could imply a

restriction to the extrafibrillar volume where MLs reside. Since CFs are held together in the bone matrix by glycosaminoglycan (GAG) chains [64], lower interfibrillar distance could mean a reduction in the bridging capability of GAGs that keep CFs in a hexagonal close packing register. Loss of GAG content in aging human bone is related to bone toughness [12]. In general, the above observations lead to a model of osteoporotic bone where the hexagonally-packed CFs are closer together than in healthy bone, restricting the extrafibrillar space that holds a majority of the mineral phase, the apatite poly-crystals (MLs), which are also significantly thicker than the MLs in control samples.

2.6 Conclusions

We presented a method to visualize and quantify several ultrastructural features of osteoporotic bone, using BF TEM imaging of FIB sectioned lift-outs. The micrographs were analyzed by a histomorphometric method applied to the nanoscale, which we term nanomorphometry. This work contributed to advance bone nanostructural research in two ways: First, it demonstrated the effectiveness of FIB to prepare sections of human bone for TEM imaging. Second, it compared multiple ultrastructural features from TEM micrographs between osteoporotic, healthy, and drug-treated bone using an unbiased image analysis workflow, and found significant differences in mineral lamella thickness (+12% in OP and OP +BP-treated compared to control) and interfibrillar distance (-21% in OP compared to control), effects that have previously been postulated using other nanostructural techniques for bone but have never before been directly imaged. Our results suggest that OP brings about an altered mineral morphology and bone matrix maturation based on increased ML thickness and reduced distance between CFs, that in the future could be studied using diffraction, spectroscopy and nanomechanical testing via a tensile specimen stage within the transmission electron microscope. The clear nanomorphometric differences could represent a new bioindicator for OP and aid in disease diagnosis. Bisphosphonate drug treatments did not appear to restore mineral lamella thickness but did appear to restore interfibrillar distance to “normal” values. This work represents a proof-of-concept that TEM can be applied to investigate ultrastructural differences indicative of OP. In future work, larger sample groups with a wider range of anti-osteoporotic treatments could be tested to determine changes in nanoscale mineralization and the effectiveness of these therapies at restoring bone ultrastructural quality.

2.7 Acknowledgements

This project was funded by the Labarge Centre for Mobility in Aging and the McMaster Institute for Research in Aging. We gratefully acknowledge the technical assistance of Travis Casagrande for preparing FIB lift-outs. Microscopy was performed at the Canadian Centre for Electron Microscopy (CCEM) at McMaster University.

Chapter 3:

Nanoscale Bone Quality at Osteoporotic Human Bone Fracture Sites Investigated by Ion Milling and BF-TEM Nanomorphometry

3.1 Abstract

Osteoporosis leads to deterioration of bone structure on the macroscale, contributing to weakening of the bone. However, the way that osteoporosis affects human bone material properties on the smallest length scales (< 1 μm^3) is not well known due to difficulty in preparing sections for transmission electron microscopy (TEM) which preserve the structure at this scale. Ion-beam milling allows investigation of the structure of bone as it would appear in its native state at this scale. In this study, we employ broad ion-milling to prepare sections of for TEM imaging. Using nanomorphometry, a nanoscale analogue to histomorphometry, we observe a significant difference in the thickness of crystalline mineral particles of apatite between control (6.0±2.0 nm) and osteoporotic (6.7±1.6 nm) bone sections, similar to differences in thickness in bone mineral crystals observed by others using small-angle x-ray scattering (SAXS). The mineral lamella thickness correlated better with donor BMD ($R^2 = 0.61$) than with the donor age ($R^2 = 0.42$). There were no significant differences in other nanomorphometric variables.

3.2 Introduction

The human skeleton is made of bone, a structurally hierarchical (multi-level organization) biomaterial that supports loads enforced on the skeleton at different angles and magnitudes. It is largely due to this nested structural organization that bone can resist micro-damage & fractures from principal axes of loading on the whole bones. However, there are still regions in our skeleton that are more susceptible to fracture, and this is especially evident as bone quality is reduced due to degenerative bone diseases, such as osteoporosis. Currently, the standard clinical diagnostic method for osteoporosis is the dual-energy X-ray absorptiometry (DEXA) scan which analyzes the mineral density of a patient's whole body, whole bone or isolated region in a bone, and is then compared to the mean BMD for the patient's age & sex group (Z-score) or to the mean BMD for a healthy adult (T-score). The latter is more commonly used as any difference observed is more pronounced. A T-score of more than -2.5 standard deviations (SD) away from

the healthy adult mean BMD entails an osteoporotic pathology [1]. Intervention may be necessary to prevent osteoporotic fractures, which have a high risk for mortality in older adults.

Osteoporotic fractures refer to fractures sustained in the vertebral, forearm or hip regions. The human femoral neck and the proximal femur in general is a common site of osteoporotic fractures, often arising from low impact falls in the elderly. Low bone mineral density at the femoral neck in women is a strong predictor of hip fracture [65]. The 10-year probability of sustaining an osteoporotic fracture in the femoral neck increases significantly both with increasing age and decreasing BMD, and the effect is accelerated in women versus men [51]. Under pre-menopausal conditions, osteoclasts are inhibited by estrogen, which induces osteoclast apoptosis [66]. In post-menopausal women, decline in estrogen causes increased osteoclastic bone resorption that is unmatched by bone formation by osteoblasts, resulting in rapid bone loss. In osteoporotic patients, thinning of trabeculae and cortices occurs, causing increased porosity due to "trabecularization" of cortical bone [30]. Hence, patients with low BMD are often prescribed anti-resorptive and/or anabolic therapies to return the BMD to healthy levels. However, the loss and gain of bone mineral reported by DEXA is observed on the micro- to macro-levels of bone structure. How the mineral structural component of bone is also affected by osteoporosis on the nanometer scale, and the implications for the quality of the bone material, is largely under-studied.

At the smallest structural scale, bone consists of tropocollagen triple-helices that assemble into 50 nm diameter, several hundred nm long collagen fibrils (CFs) as well as carbonated apatite (calcium phosphate) nanocrystals that form approximately 5 nm thick, 60 nm wide, 100-200 nm long polycrystalline assemblies termed "mineral lamellae" (MLs) between the CFs [3], [38]. The MLs mineralize interfibrillarly in the form of stacks, with the *c* axis of the crystals aligned with the length of the CF. These characteristics were measured from bright-field and dark-field transmission electron microscopy imaging which is capable of sub-nanometer resolution. It has been shown through a variety of techniques that probe the nanoscale bone quality in human bone that the mineral phase of bone is significantly affected by degenerative bone disease such as osteoporosis, in both composition [19], [20], [22], [53], [54], [67] and structural morphology [16], [17]. However, these techniques measure average nanoscale characteristics using micrometer- scale probes. Osteoporotic bone ultrastructure has rarely been

imaged directly at the nanoscale using transmission electron microscopy, [41], [68]. A major complication in previous studies of bone ultrastructure is the use of an ultramicrotome to section bone for TEM. Although a rapid method to prepare electron-transparent bone specimens, the diamond blade of the ultramicrotome has been shown to break MLs, altering the mineral lamellae framework when viewed in TEM [4]. By comparison, ion-beam milling, which thins the bone specimen by eroding the surface with argon ions, leaves the bone ultrastructure intact, and should be the method of choice for bone sample preparation for TEM [3], [5], [37], [61]. In the current study, we use TEM to image the bone ultrastructure directly and use nanomorphometry (as in Chapter 2) to measure and compare dimensions of ultrastructural components in an effort to understand the effects of post-menopausal osteoporosis on human bone from the nanometer-scale upwards.

3.3 Materials & Method

Specimens: Samples of human bone were provided by Dr. Cheryl Quenneville (Mechanical Engineering, School of Biomedical Engineering, McMaster University, ON). Two osteoporotic and three control proximal femurs were taken post-mortem from donors with ethics board approval and had undergone biomechanical testing. They were selected based on fracture location and bone mineral density (BMD) (Table 1).

Table 3.1: Human post-mortem donor proximal femurs selected for sectioning and preparation by ion milling for BF-TEM nanomorphometry

Group	Age / Sex	T-score
Control	57 / F	-0.1
	70 / F	-0.9
	73 / F	-0.8
Osteoporotic	76 / F	-3.0
	85 / F	-2.7

Sample preparation: A Dremel saw and hand saw were used to cut pieces of the medial inferior femoral neck from each proximal femur (Figure 3.1). Each bone fragment was placed into a separate glass jar containing 4% glutaraldehyde fixative in 0.1 M sodium cacodylate buffer for 7 days.

Figure 3.1: Human proximal femur (adapted from [69]) with the medial inferior femoral neck outlined in the dashed red box, which was the location selected for extraction by Dremel saw and hand saw from the bulk bone biomaterial of each control and osteoporotic proximal femur. White dotted box shows two example section planes by low-speed saw after fixing. Cut pieces included cortical and trabecular bone.

A 1 millimeter thick section of bone was cut from each piece of bone, perpendicular to the long axis of the femoral neck using a Buehler Isomet Low-Speed Saw with a diamond-edge wafering blade. The sections were dehydrated for 24 hours in graded ethanol solutions (70% to 100%, increasing 10% each grade), air dried, and embedded in Epotek 353ND resin in a polystyrene cuvette. The resin-embedded samples were cured for 24 hours at room temperature, and then at 60 °C for 1 hour. Using the low-speed saw, a 0.5 mm section was cut from the cuvette material, and attached to a hand polishing tool with ethyl cyanoacrylate. The bone sections were then successively polished on both sides with a series of silicon carbide polishing papers (FEPA 500, 800, 1200, 2000, 4000) until each section was roughly 150 µm thick as measured with a Mitutoyo digital thickness gauge. Each section was then imaged by a Nikon SMZ-1000 light stereomicroscope to find trabecular or trabecularized regions of interest (ROI)

for mounting. A 3 mm diameter disc was removed from the thinned section using a manual hole punch, and mounted on a copper or molybdenum sample ring with 3 mm external and 2 mm internal diameter. It was then thinned on both sides to below 50 µm thickness using 3-5 µm diamond paste on a Gatan dimple grinder.

Ion milling thin bone sections: Each section was ion milled on a Fischione 1010 low-angle liquid-nitrogen-cooled ion mill for 4-6 hours using a 6-7° milling angle, depending upon the thickness of the material, until a hole formed near the center of the sample. The samples were then coated with a 50 Å thick layer of carbon to act as a sacrificial layer to the electron beam.

Bright field transmission electron microscopy imaging: Imaging was performed on a JEOL 2010F Scanning Transmission Electron Microscope in bright-field mode, using 200 kV accelerating voltage and dual-axis tilting stage. The samples were imaged at low magnifications (40,000x-100,000x) to obtain overviews and high magnifications (300,000x-1,500,000x) to capture detailed views of bone ultrastructural features. ROIs included sections oriented normal to the CF axes (cross-sectional regions, CSRs) and parallel to the CF axes (longitudinal regions, LRs) (Figure 3.2), as well as some oblique views of these two orientations. Only cross-sections were used in the nanomorphometry analysis.

Blinded nanomorphometry of nanoscale bone quality indicators: The images, in Digital Micrograph (.DM3) format, were converted to .TIF, preserving the scale of the images. A blinding algorithm (BlindAnalysis.ijm) for Fiji/ImageJ [60] was used to remove all associable labels from the images, which were stored in a log file. They were analyzed using nanomorphometric techniques described in Chapter 2. The following bioindicators of the collagen fibrils and mineral lamellae components were measured: collagen fibril diameter (major and minor axes; as the minor axis describes the "true" diameter in cases of tilted CFs), interfibrillar distance, mineral lamella thickness and mineral lamella stack thickness. Dimensions of these features were recorded using the line tool in Fiji/ImageJ. The precision of analysis of each dimension in high magnification BF-TEM images was ± 0.5 nm. The results of each analysis were recorded, and the images unblinded using the log file. Data were organized based on the bone sample group (control or osteoporotic).

Statistical analysis: Power analysis on a training dataset determined that >120 measurements of mineral lamella thickness and >50 measurements for other indicators were required to achieve

>80% power in each group (control and osteoporotic). Significance was determined through statistical testing in all cases using a t-test ($p<0.05$) with Welch's correction.

3.4 Results

Figure 3.2 shows typical TEM images obtained of cross-sectional and longitudinal regions in bone ultrastructure. These images are similar to images of bone ultrastructure from previous works using both ion milling and focused ion beam (FIB) preparation methods. Although in ion milling it is necessary to erode a hole in the section to be sufficiently electron-transparent, this process does not appear to affect the ultrastructure of the bone; MLs which are few nm away from the hole maintain their shape within their bone matrix.

Table 3.2 below shows results of nanomorphometry for all bioindicators studied. Differences in collagen fibril diameter and interfibrillar distance were non-significant.

Table 3.2: Bone ultrastructure nanomorphometry of control and osteoporotic human bone ion milled sections.

Bioindicator	**Control Bone**	**Osteoporotic Bone**
Mineral lamella thickness	6.0 ± 2.0 nm	6.7 ± 1.6 nm *
Mineral lamella stack thickness	26.4 ± 10 nm	28.3 ± 8.8 nm
Collagen fibril minor diameter	35.2 ± 8.3 nm	35.9 ± 8.6 nm
Interfibrillar distance	77 ± 23 nm	82 ± 26 nm

*Significant difference found by t-test with Welch's correction ($p<0.05$)

The only bioindicator to reach statistical significance between control and osteoporotic bone was the mineral lamella thickness, which measured 6.0 ± 2.0 nm in control specimens and 6.7 ± 1.6 nm in osteoporotic specimens (Figure 3.3) corresponding to a 12% difference. The ML thickness was plotted against specimen donor age and proximal femur T-score in Figure 3.4.

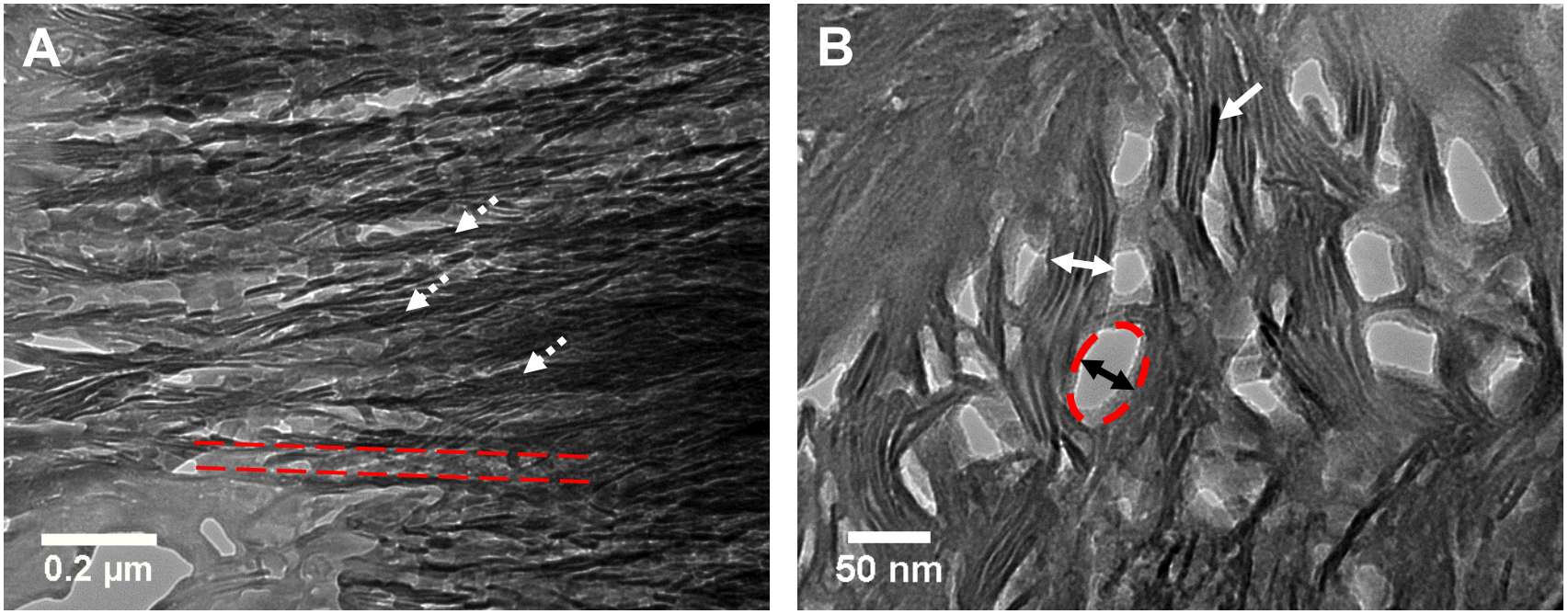

Figure 3.2: ROIs imaged by BF-TEM in ion milled human bone sections for use in nanomorphometry. A) Longitudinal region showing vertical banding pattern of the gap-overlap periodicity of collagen fibrils (lying horizontally in the plane of the image), that appear as lanes (red dashed lines) in between stacks of MLs (dashed white arrows) viewed length-wise across the image plane. B) Cross-sectional region showing light contrast "holes" that are the sites of collagen fibrils (likely milled away by the ion mill) whose long axis is normal to the image plane. Red dashed circle shows the typical diameter of a collagen fibril that is slightly eccentric, in which case the minor diameter (black double-headed arrow) gives the true diameter. MLs appear as dark contrast crystals (white solid arrow) within stacks several MLs thick (white double-headed arrow) which curve around adjacent collagen fibrils.

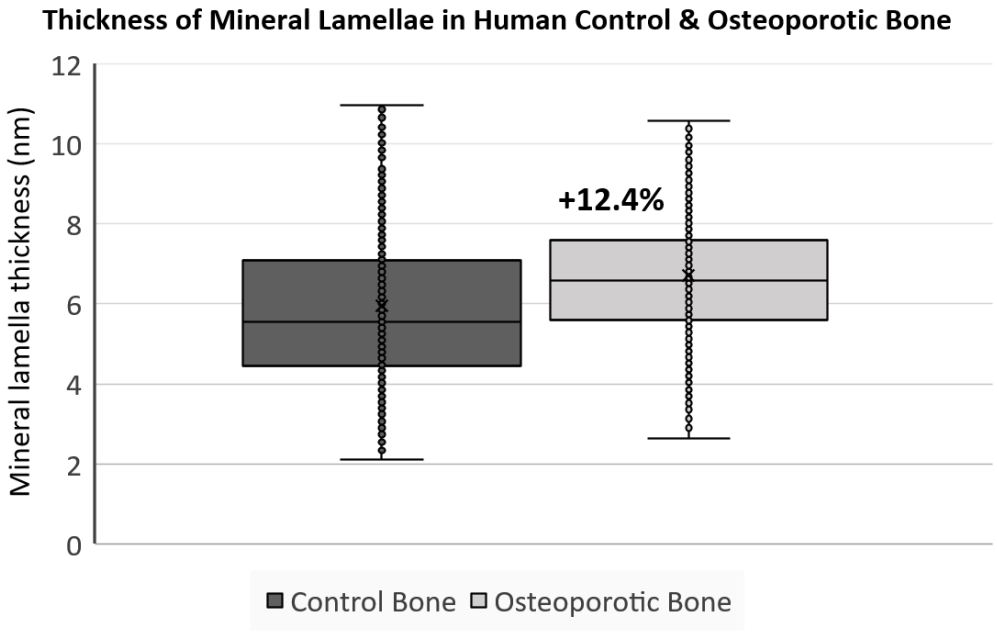

Figure 3.3: Results of nanomorphometry of ML thickness in control and osteoporotic ion-milled bone sections, shown as quartiles of data in a box-and-whisker plot (median = middle line of box; mean = X). The mean control ML thickness was 5.96 ± 2.07 nm for control bone and 6.70 ± 1.58 nm for osteoporotic bone. Osteoporotic bone had a significant increase in the mean ML thickness of 12.4 %.

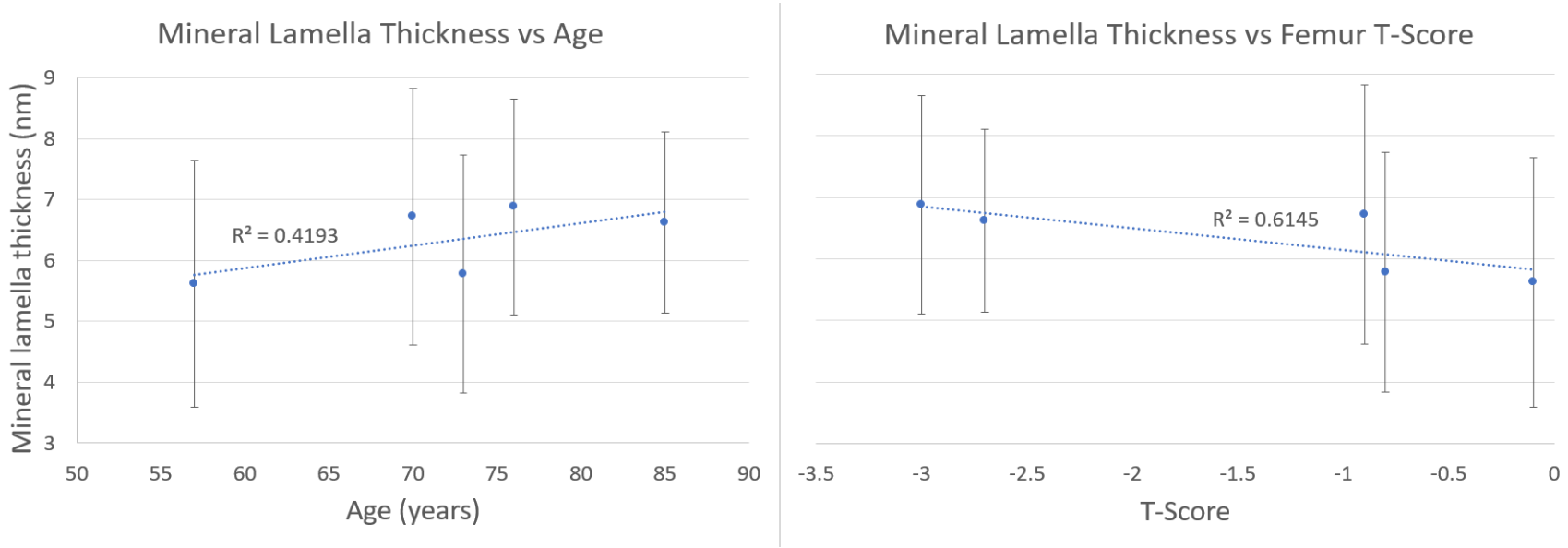

Figure 3.4: Average mineral lamella thickness in each specimen studied as a function of A) donor age, and B) proximal femur T-score. Points represent average ML thickness measured within an individual bone specimen. A) ML thickness increases as age of the donor increases. B) ML thickness increases as T-score decreases, that is, as the femoral donor becomes more osteoporotic. The linear trendline correlates better when comparing ML thickness and T-score, as seen by the higher coefficient of determination (R^2).

3.5 Discussion

The only significant nanomorphometric difference that we observed was a 12% increase in thickness of mineral lamellae in OP bone compared with controls. Similar differences have been previously reported in ovariectomized rats, a model for post-menopausal osteoporosis, using small-angle X-ray scattering (SAXS) [16], [17]. Mathavan et al found that mineral lamella thickness increased by 7.8 % between control and ovariectomized (OVX) osteoporotic rat bone [17]. Valenta et al also found an identical result (7.1 % increase in mineral lamella thickness from non-OVX to OVX rat bone). However, SAXS measurements of the thickness of mineral lamellae in bone are, for some reason, consistently smaller than what we observe here and in other TEM studies [5], [11], [61]. The ML thickness measured by SAXS is reported to be around 2.2-2.6 nm [16], [17], [26]. The thickness of the mineral lamellae measured in this study agree with the reported values measured in previous TEM studies, even the observation of large MLs greater than 8 nm [11]. However, the percentage increase of ML thickness between control and osteoporotic human bone observed in this study is similar to that observed with SAXS.

Previously reported values for CF diameter in human bone cross-sectional ultrastructure using nanomorphometry in TEM report 36.3 nm as the minor axis diameter [5], which agrees with the average CF diameter measured in control and OP bone in this study. These values are significantly smaller than those reported for cross-sectional collagen fibrils in unmineralized osteoid (50-60 nm) [70], and also collagen fibrils measured in longitudinal orientation (50-55 nm) [5], [11] in TEM. The difference is more likely than not from the non-uniformity and superposition of ML stacks surrounding the CFs in cross-sectional orientation. In addition, the border of MLs and unstained CFs in TEM is visualized variably between image analysts. This makes accurate nanomorphometric analysis of CF diameter in mineralized bone tissue difficult.

The relevance of the thickening of the crystals to the development of post-menopausal and/or old-age osteoporosis is not clear. Some authors suggest that thicker crystals result due to their growth in the secondary mineralization phase [16], [17], and thus the thickness is dependent on the age/maturity of the bone tissue. To test this theory, the ML thickness was plotted first as a function of age, and second as a function of BMD (shown in Figure 3.4). There appears to be a trend of increasing ML thickness with age but the correlation ($R^2 = 0.42$) is not significant. There is also a trend for ML thickness to decrease with BMD but the correlation ($R^2 = 0.61$) was not

significant ($p<0.05$). Unfortunately, in this study we were provided with no information about possible use of anti-osteoporosis therapies by the study subjects, which may account for increased variability.

This is the first study to employ ion milling, TEM and nanomorphometric image analysis to study differences in bone ultrastructure between control and osteoporotic human bone. It appears that mineral lamella thickness could be included as a nanoscale bioindicator of human osteoporosis although sample preparation and obtaining *ex-vivo* samples from patients would be a challenge.

3.6 Conclusions

This pilot nanomorphometric study of changes in the ultrastructure of bone from a common osteoporotic fracture site in the proximal femur, found no significant differences between OP and controls in collagen fibril diameter, interfibrillar distance, or stack thickness. However, there was a significant difference in thickness of mineral lamellae with MLs in osteoporotic bone specimens being significantly thicker (6.7 ± 1.6 nm) than in control specimens (6.0 ± 2.0 nm). The ML thickness correlated positively with age, negatively with BMD, and had a greater correlation with the donor BMD ($R^2 = 0.61$) than with the donor age ($R^2 = 0.42$). Although the percent difference in thickness of mineral lamellae observed in our study was comparable to that obtained in SAXS studies, the magnitude of the thicknesses observed by us was significantly larger than that observed by SAXS. The thickness of MLs observed by us is consistent with estimates of the thickness of apatite crystals in bone observed in many other studies and suggests that, for some reason, the SAXS technique underestimates this thickness. Correlating these results to recorded fracture toughness in the future [71] would be useful to determine if the size of mineral lamellae affects mechanical properties.

3.7 Acknowledgements

Funding for this project was provided by the Labarge Centre for Mobility in Aging and the McMaster Institute for Research in Aging. Ion milling and TEM was performed at the Canadian Centre for Electron Microscopy (CCEM) at McMaster University.

Chapter 4: Summary & Future Directions

4.1 Summary

Osteoporosis is a multifactorial degenerative bone disease whose effects have been detected on multiple length scales using a variety of techniques that probe bone quality. This work specifically investigated the nanoscale quality of human osteoporotic bone ultrastructure using a blinded histomorphometric method applied to TEM images of bone tissue, which we term *nanomorphometry*. Four structural features of human bone ultrastructure were analyzed: CF diameter, interfibrillar distance, ML thickness, and ML stack thickness. Two different cohorts of bone material donors from osteoporotic patients and their age-matched controls were prepared for BF-TEM imaging.

Chapter 2 studied a sample cohort consisting of bone material extracted during an intertrochanteric nail fixation procedure. Patients (post-menopausal women) either had no fracture (biopsy performed instead), fracture but no previous drug-treatment, or fracture with a history of bisphosphonate use. The samples were imaged by optical microscopy and SEM to compose a detailed mosaic of the sample micro-architecture, density and topology of (hemi-/) osteonal lamellar layers. FIB milling was then used to extract a lift-out from a trabecular or "trabecularized" (enlarged cortical) region of bone that spanned multiple osteonal layers. Nanomorphometry revealed that the crystalline apatite mineral lamellae were significantly thicker in osteoporotic bone, whether BP-treated or not, than in control bone. Interfibrillar distance was significantly reduced in osteoporotic bone but was returned to control levels in BP-treated osteoporotic bone. This study suggests that osteoporotic fracture incidence, a major risk factor of osteoporosis, is correlated to changes in the structure of bone on the nanoscale not only the microscale. Bisphosphonates may be able to return the bone ultrastructure to control levels; however their effect should be compared to anabolic drugs that promote new bone formation to discern their effect on the recovery of the nanoscale structure.

In Chapter 3, bone biomaterial from proximal femurs (the medial inferior femoral neck) of a post-menopausal osteoporotic donor cohort was studied. A method to extract, section, polish and ion mill post-mortem human bone from bulk specimens was successful in producing large, electron-transparent fields of view of bone ultrastructure in trabecular and trabecularized

endocortical sites. Nanomorphometry of ion milled samples revealed that ML thickness is significantly increased in osteoporotic bone than in age-matched controls. No other nanoscale bioindicator between the two groups reached statistical significance ($p < 0.05$). Proximal femur BMD, measured by DEXA, correlated negatively with ML thickness, while donor age correlated positively; however, neither correlation was significant. This study demonstrated the increase in mineral lamella thickness as a potential bioindicator for post-menopausal osteoporosis.

4.2 Limitations

The study results presented herein are limited by several factors. First, the sizes of sample groups (control, osteoporotic and OP drug-treated) were too small for convincing statistical significance or correlation of nanomorphometric measures. Nonetheless, this limitation was balanced with high statistical power of bioindicators measured, as well as blinded image analysis design. Second, the preparation of electron transparent ion milled samples for TEM is either expensive (with FIB) or lengthy (with broad ion beam milling), which prevents high-throughput analysis of many samples. However, ion milling is necessary to keep the bone ultrastructure intact to perform nanomorphometric measurements on TEM micrographs. Third, although care was taken to analyze images from different regions of the specimen, the small physical size of the samples extracted may not be representative of osteoporotic bone as a whole; nevertheless, anatomical regions of the skeleton thought to be most affected by osteoporosis were selected in an effort to focus the study on osteoporotic bone, and not necessarily an osteoporotic whole bone or patient. Fourth, there may exist user error between image analysis operators as there is some subjectivity to the selected nanomorphometric measures. The error was minimized by using one image analyst for the entire project. User error may have also presented in the misinterpretation of tilt or contrast effects which would influence a manual measurement. Hence, there may be some inherent variability in the nanomorphometric results reported.

4.3 Future Directions

The present study established and developed the *nanomorphometry* method as a viable image analysis technique of BF-TEM micrographs to discern significant differences in osteoporotic versus control bone ultrastructure; the method used a blinded manual operator to analyze nanoscale bioindicators in the micrographs. A major focus of future work in this field will be the development of an automated image analysis method to detect and measure the

morphology of mineral particles and other ultrastructural features in an image. This will enable instrumental analysis of a large set of images and further reduce bias in image analysis. Larger sample cohorts of osteoporotic and control bone from human donors or osteoporotic animal models will be required to validate the ultrastructural differences observed in this work. There should be inclusion of study subjects and data on past anti-resorptive and anabolic drug-treatments.

The FIB lift-out and ion milling methods are inherently destructive to the surrounding bone material, as they mill it away, and should thus be applied near the end of the bone material analysis. Correlative studies using a combination of techniques such as SEM, FTIRM and SAXS can be used beforehand to obtain complementary data on nanoscale compositional and structural bone quality. Then, ion milling, TEM and nanomorphometry in a specific ROI can be performed. In this way, the bioindicator signals obtained individually from each technique can be consolidated to determine how indicators of mineralization, for example, measured on the microscale, translate to differences in ultrastructural features, or the other way around.

The nanoscale chemical composition of mineral lamellae and collagen fibrils in osteoporotic bone can be studied in the TEM using electron energy loss spectroscopy (EELS) to determine whether compositional differences in the crystalline apatite mineral lamellae exist compared to controls. High-resolution TEM (HR-TEM) could also be employed to analyze the nature of the curvature of mineral lamellae, or their internal structure, especially of very thick (>10 nm) MLs.

The results presented through this project were beneficial for defining osteoporotic bone through a potential bioindicator of nanostructural quality, the mineral lamella thickness. The increased ML thickness in osteoporotic bone suggests that there is a fundamental difference in the structure of osteoporotic bone on the nanoscale. Whether other anti-osteoporotic therapies promote “healthy” mineral morphology and how altered mineral morphologies affect bone strength are important topics to understand to track effective therapies and the associated reduction in fracture risk they afford the patient. An altered bone structure on the nanoscale has crucial implications for the design of patient-specific bone implants which have high degree of integration with bone across many hierarchical length scales.

References

[1] WHO Study Group, "Assessment of Fracture Risk and its Application to Screening for Postmenopausal Osteoporosis," *Word Health Organization technical reports series*, vol. 843. pp. 1–136, 1992.

[2] G. M. Blake and I. Fogelman, "The role of DXA bone density scans in the diagnosis and treatment of osteoporosis," *Postgrad. Med. J.*, vol. 83, no. 982, pp. 509–517, 2007.

[3] H. P. Schwarcz, "The ultrastructure of bone as revealed in electron microscopy of ion-milled sections," *Semin. Cell Dev. Biol.*, vol. 46, pp. 44–50, 2015.

[4] V. Jantou, M. Turmaine, G. D. West, M. A. Horton, and D. W. Mccomb, "Focused ion beam milling and ultramicrotomy of mineralised ivory dentine for analytical transmission electron microscopy," *Micron*, vol. 40, pp. 495–501, 2009.

[5] E. A. McNally, H. P. Schwarcz, G. A. Botton, and A. L. Arsenault, "A model for the ultrastructure of bone based on electron microscopy of ion-milled sections," *PLoS One*, vol. 7, no. 1, pp. 1–12, 2012.

[6] H. P. Schwarcz, D. Abueidda, and I. Jasiuk, "The Ultrastructure of Bone and Its Relevance to Mechanical Properties," *Front. Phys.*, vol. 5, no. September, 2017.

[7] Y. Li and C. Aparicio, "Discerning the Subfibrillar Structure of Mineralized Collagen Fibrils: A Model for the Ultrastructure of Bone," *PLoS One*, vol. 8, no. 9, pp. 1–12, 2013.

[8] S. Morgan, A. A. Poundarik, and D. Vashishth, "Do Non-collagenous Proteins Affect Skeletal Mechanical Properties?," *Calcif. Tissue Int.*, vol. 97, no. 3, pp. 281–291, 2015.

[9] F. Nudelman *et al.*, "The role of collagen in bone apatite formation in the presence of hydroxyapatite nucleation inhibitors," *Nat. Mater.*, vol. 9, no. 12, pp. 1004–1009, 2010.

[10] M. Giraud-Guille, "Twisted plywood architecture of collagen fibrils in human compact bone osteons," *Calcif. Tissue Int.*, vol. 42, pp. 167–180, 1988.

[11] H. P. Schwarcz, E. A. McNally, and G. A. Botton, "Dark-field transmission electron microscopy of cortical bone reveals details of extrafibrillar crystals," *J. Struct. Biol.*, vol. 188, pp. 240–248, 2014.

[12] X. Wang *et al.*, "Age-Related Deterioration of Bone Toughness Is Related to Diminishing Amount of Matrix," *JBMR Plus*, vol. 2, no. 3, pp. 164–173, 2018.

[13] H. Fonseca, D. Moreira-Gonçalves, H.-J. Appell Coriolano, and J. Alberto Duarte, "Bone Quality : The Determinants of Bone Strength and Fragility," *Sport. Med*, vol. 44, pp. 37–53, 2014.

[14] J. Compston, "Bone quality: what is it and how is it measured?," *Arq. Bras. Endocrinol. Metabol.*, vol. 50, no. 4, pp. 579–585, 2006.

[15] P. Roschger, B. Misof, E. Paschalis, P. Fratzl, and K. Klaushofer, "Changes in the degree of mineralization with osteoporosis and its treatment," *Curr. Osteoporos. Rep.*, vol. 12, no. 3, pp. 338–350, 2014.

[16] A. Valenta *et al.*, "Combined treatment with PTH (1-34) and OPG increases bone volume and uniformity of mineralization in aged ovariectomized rats," *Bone*, vol. 37, no. 1, pp. 87–95, 2005.

[17] N. Mathavan, M. J. Turunen, M. Tägil, and H. Isaksson, "Characterising bone material composition and structure in the ovariectomized (OVX) rat model of osteoporosis," *Calcif. Tissue Int.*, vol. 97, no. 2, pp. 134–144, 2015.

[18] A. L. Boskey *et al.*, "Examining the Relationships between Bone Tissue Composition, Compositional Heterogeneity and Fragility Fracture: A Matched Case Controlled FTIRI Study," *J Bone Min. Res*, vol. 31, no. 5, pp. 1070–1081, 2016.

[19] S. Gamsjaeger, R. Mendelsohn, A. L. Boskey, S. Gourion-Arsiquaud, K. Klaushofer, and E. P. Paschalis, "Vibrational spectroscopic imaging for the evaluation of matrix and mineral chemistry," *Curr. Osteoporos. Rep.*, vol. 12, no. 4, pp. 454–464, 2014.

[20] E. P. Paschalis, R. Mendelsohn, and A. L. Boskey, "Infrared assessment of bone quality: A review," *Clin. Orthop. Relat. Res.*, vol. 469, no. 8, pp. 2170–2178, 2011.

[21] M. Saito and K. Marumo, "Collagen cross-links as a determinant of bone quality: A possible explanation for bone fragility in aging, osteoporosis, and diabetes mellitus," *Osteoporos. Int.*, vol. 21, no. 2, pp. 195–214, 2010.

[22] M. M. Kłosowski *et al.*, "Electron Microscopy Reveals Structural and Chemical Changes at the Nanometer Scale in the Osteogenesis Imperfecta Murine Pathology," *ACS Biomater. Sci. Eng.*, vol. 3, no. 11, pp. 2788–2797, 2017.

[23] A. A. Lloyd *et al.*, "Atypical fracture with long-term bisphosphonate therapy is associated with altered cortical composition and reduced fracture resistance," *Proc. Natl. Acad. Sci.*, p. 201704460, 2017.

[24] Z. X. Wang, A. A. Lloyd, J. C. Burket, S. Gourion-Arsiquaud, and E. Donnelly, "Altered distributions of bone tissue mineral and collagen properties in women with fragility fractures," *Bone*, vol. 84, pp. 237–244, 2016.

[25] M. Georgiadis, R. Müller, and P. Schneider, "Techniques to assess bone ultrastructure organization: Orientation and arrangement of mineralized collagen fibrils," *Journal of the Royal Society Interface*, vol. 13, no. 119. 2016.

[26] N. P. Camacho, S. Rinnerthaler, E. P. Paschalis, R. Mendelsohn, A. L. Boskey, and P. Fratzl, "Complementary Information on Bone Ultrastructure From Scanning Small Angle X-ray Scattering and Fourier-transform Infrared Microspectroscopy," *Bone*, vol. 25, no. 3, pp. 287–293, 1999.

[27] P. D. Delmas and E. Seeman, "Changes in bone mineral density explain little of the reduction in vertebral or nonvertebral fracture risk with anti-resorptive therapy," *Bone*, vol. 34, no. 4, pp. 599–604, 2004.

[28] T. Topoliński, A. Mazurkiewicz, S. Jung, A. Cichański, and K. Nowicki, "Microarchitecture parameters describe bone structure and its strength better than BMD," *Sci. World J.*, vol. 2012, 2012.

[29] J. C. Crockett, M. J. Rogers, F. P. Coxon, L. J. Hocking, and M. H. Helfrich, "Bone remodelling at a glance," *J. Cell Sci.*, vol. 124, no. 7, pp. 991–998, 2011.

[30] R. M. D. Zebaze *et al.*, "Intracortical remodelling and porosity in the distal radius and post-mortem femurs of women : a cross-sectional study," *Lancet*, vol. 375, pp. 1729–1736, 2010.

[31] M. T. Drake, B. L. Clarke, and S. Khosla, "Bisphosphonates: Mechanism of Action and

Role in Clinical Practice," *Mayo Clin Proc*, vol. 83, no. 9, pp. 1032–1045, 2008.

[32] T. Seno *et al.*, "Once-weekly teriparatide improves glucocorticoid-induced osteoporosis in patients with inadequate response to bisphosphonates," *Springerplus*, vol. 5, no. 1, 2016.

[33] R. K. Nalla, A. E. Porter, C. Daraio, A. M. Minor, and V. Radmilovic, "Ultrastructural examination of dentin using focused ion-beam cross-sectioning and transmission electron microscopy," *Micron*, vol. 36, pp. 672–680, 2005.

[34] K. Grandfield, A. Palmquist, H. Engqvist, and P. Thomsen, "Resolving the CaP-bone interface," *Biomatter*, vol. 2, no. 1, pp. 15–23, 2012.

[35] V. Jantou-Morris, M. A. Horton, and D. W. McComb, "The nano-morphological relationships between apatite crystals and collagen fibrils in ivory dentine," *Biomaterials*, vol. 31, no. 19, pp. 5275–5286, 2010.

[36] O. A. Tertuliano and J. R. Greer, "The nanocomposite nature of bone drives its strength and damage resistance," *Nat. Mater.*, vol. 15, no. 11, 2016.

[37] K. Grandfield, V. Vuong, and H. P. Schwarcz, "Ultrastructure of Bone: Hierarchical Features from Nanometer to Micrometer Scale Revealed in Focused Ion Beam Sections in the TEM," *Calcif. Tissue Int.*, vol. 103, no. 6, pp. 606–616, 2018.

[38] A. L. Arsenault and M. D. Grynpas, "Crystals in Calcified Epiphyseal Cartilage and Cortical Bone of the Rat," *Calcif. Tissue Int.*, vol. 43, pp. 219–225, 1988.

[39] W. J. Landis and K. J. Hodgens, "Mineralization of Collagen May Occur on Fibril Surfaces : Evidence from Conventional and High-Voltage Electron Microscopy and Three-Dimensional Imaging," vol. 117, pp. 24–35, 1996.

[40] S. Lees, K. S. Prostak, V. K. Ingle, and K. Kjoller, "The Loci of Mineral in Turkey Leg Tendon As Seen By Atomic Force Microscope and Electron Microscopy," *Calcif. Tissue Int.*, vol. 55, pp. 180–189, 1994.

[41] E. I. Suvorova, P. P. Petrenko, and P. A. Buffat, "Scanning and transmission electron microscopy for evaluation of order/disorder in bone structure," *Scanning*, vol. 29, no. 4, pp. 162–170, 2007.

[42] R. F. Egerton, "Mechanisms of Radiation Damage in Beam-Sensitive Specimens , for TEM Accelerating Voltages Between 10 and 300 kV," *Microsc. Res. Tech.*, vol. 75, pp. 1550–1556, 2012.

[43] D. B. Williams and C. B. Carter, "Transmission electeron microscopy," in *Transmission Electron Microscopy Part 1: Basics*, 2nd Editio., Springer, 2009, p. 804.

[44] D. B. Williams and C. B. Carter, "Bright-Field and Dark-Field Imaging," in *Transmission Electron Microscopy Part 1: Basics*, 2nd Editio., Springer, 2009.

[45] J. Schindelin *et al.*, "Fiji: an open-source platform for biological-image analysis," *Nat. Methods*, vol. 9, pp. 676–682, 2012.

[46] B. Erickson, M. Fang, J. M. Wallace, B. G. Orr, C. M. Les, and M. M. B. Holl, "Nanoscale Structure of Type I Collagen Fibrils: Quantitative Measurement of D-spacing," *Biotechnol J*, vol. 8, no. 1, pp. 117–126, 2013.

[47] B. Alexander *et al.*, "The nanometre-scale physiology of bone: Steric modelling and scanning transmission electron microscopy of collagen-mineral structure," *J. R. Soc. Interface*, vol. 9, no. 73, pp. 1774–1786, 2012.

[48] E. McNally, F. Nan, G. A. Botton, and H. P. Schwarcz, "Scanning transmission electron microscopic tomography of cortical bone using Z-contrast imaging," *Micron*, vol. 49, pp. 46–53, 2013.

[49] N. Reznikov, R. Shahar, and S. Weiner, "Bone hierarchical structure in three dimensions," *Acta Biomater.*, vol. 10, no. 9, pp. 3815–3826, 2014.

[50] E. Hamed, E. Novitskaya, J. Li, P.-Y. Chen, I. Jasiuk, and J. McKittrick, "Elastic moduli of untreated, demineralized and deproteinized cortical bone: Validation of a theoretical model of bone as an interpenetrating composite material," *Acta Biomater.*, vol. 8, no. 3, pp. 1080–1092, 2012.

[51] J. A. Kanis, O. Johnell, A. Oden, A. Dawson, C. De Laet, and B. Jonsson, "Ten year probabilities of osteoporotic fractures according to BMD and diagnostic thresholds," *Osteoporos. Int.*, vol. 12, no. 12, pp. 989–995, 2001.

[52] M. J. Turunen *et al.*, "Bone mineral crystal size and organization vary across mature rat bone cortex," *J. Struct. Biol.*, vol. 195, no. 3, pp. 337–344, 2016.

[53] A. L. Boskey *et al.*, "Examining the Relationships between Bone Tissue Composition, Compositional Heterogeneity, and Fragility Fracture: A Matched Case-Controlled FTIRI Study," *J. Bone Miner. Res.*, vol. 31, no. 5, pp. 1070–1081, 2016.

[54] S. Gourion-Arsiquaud *et al.*, "Use of FTIR spectroscopic imaging to identify parameters associated with fragility fracture," *J. Bone Miner. Res.*, vol. 24, no. 9, pp. 1565–1571, 2009.

[55] D. Ruffoni and G. H. van Lenthe, *Finite Element Analysis in Bone Research: A Computational Method Relating Structure to Mechanical Function, Update*, no. December. Elsevier Ltd., 2017.

[56] R. Berisio, L. Vitagliano, L. Mazzarella, and A. Zagari, "Crystal structure of the collagen triple helix model [(Pro-Pro-Gly)10]3," 2009.

[57] D. E. Ellis *et al.*, "A theoretical and experimental study of lead substitution in calcium hydroxyapatite," *Phys. Chem. Chem. Phys.*, vol. 8, pp. 967–976, 2006.

[58] H. G. Bone *et al.*, "Ten Years' Experience With Alendronate for Osteoporosis in Postmenopausal Women," *Obstet. Gynecol. Surv.*, vol. 59, no. 8, pp. 597–598, 2004.

[59] N. Reznikov, M. Bilton, L. Lari, M. M. Stevens, and R. Kröger, "Fractal-like hierarchical organization of bone begins at the nanoscale," *Science (80-.).*, vol. 360, no. 6388, 2018.

[60] S. Royle, "BlindAnalysis.ijm." .

[61] B. E. J. Lee, L. Luo, K. Grandfield, C. M. Andrei, and H. P. Schwarcz, "Identification of collagen fibrils in cross sections of bone by electron energy loss spectroscopy (EELS)," *Micron*, vol. 124, no. December 2018, 2019.

[62] A. M. Parfitt and R. R. Recker, "Bone histomorphometry: techniques and interpretation," *Physiol. Clin. Significance Bone Histomorphometric Data, CRC Press*, pp. 143–224, 1983.

[63] M. J. Turunen *et al.*, "Evaluation of composition and mineral structure of callus tissue in

rat femoral fracture," *J. Biomed. Opt.*, vol. 19, no. 2, p. 025003, 2014.

[64] J. E. Scott, "Cartilage is held together by elastic glycan strings. Physiological and pathological implications," in *Biorheology*, 2008.

[65] S. R. Cummings *et al.*, "Bone density at various sites for prediction of hip fractures. The Study of Osteoporotic Fractures Research Group.," *Lancet (London, England)*, vol. 341, no. 8837, pp. 72–5, 1993.

[66] T. Kameda *et al.*, "Estrogen Inhibits Bone Resorption by Directly Inducing Apoptosis of the Bone-resorbing Osteoclasts," *J. Exp. Med.*, vol. 186, no. 4, pp. 489–495, 1997.

[67] F. Karaaslan, M. Mutlu, M. U. Mermerkaya, S. Karaoglu, S. Sacmaci, and S. Kartal, "Comparison of bone tissue trace-element concentrations and mineral density in osteoporotic femoral neck fractures and osteoarthritis," *Clin. Interv. Aging*, vol. 9, pp. 1375–1382, 2014.

[68] O. Gül, O. Ş. Atik, D. Erdoğan, G. Göktaş, and Ç. Elmas, "Transmission and scanning electron microscopy confirm that bone microstructure is similar in osteopenic and osteoporotic patients," *Eklem Hast. ve Cerrahisi*, vol. 24, no. 3, pp. 126–132, 2013.

[69] S. H. Patel and K. P. Murphy, "Fractures of the proximal femur : correlates of radiological evidence of osteoporosis," *Skeletal Radiol.*, vol. 35, no. 4, pp. 202–211, 2006.

[70] P. Sarathchandra, F. M. Pope, and S. Y. Ali, "Morphometric analysis of type I collagen fibrils in the osteoid of osteogenesis imperfecta," *Calcif. Tissue Int.*, vol. 65, no. 5, pp. 390–395, 1999.

[71] C. Gluek, "Evaluating the Mechanical Response of Novel Synthetic Femurs Representing Osteoporotic Bone," McMaster University, 2019.

Glossary of Specialized Terms

Apatite crystal *c*-axis: The longest crystallographic axis of apatite (calcium phosphate) crystals. This is generally co-aligned with the long axis of collagen fibrils.

Bioindicator/Biomarker: Used interchangeably as a measure of a structural characteristic of which is an indicator of disease. In this thesis, biomarker or indicator refers to a structural measure from nanomorphometry of bone that can identify a difference between osteoporotic compared to control bone.

Hemi-osteon: Layers of hemi-spherical bone deposited by osteoblasts on the trabecular remodeling surface.

Ultramicrotomy: The method of using an ultramicrotome to section bone for TEM.

Ultrastructure: Used interchangeably with “nanoscale structure”, this term refers to the arrangement of bone components (collagen fibrils and mineral lamellae) on the nanometer scale.